12-16-2011

3-D Transient Hydraulic Tomography in Unconfined Aquifers with Fast Drainage Response

Michael Cardiff
Boise State University

Warren Barrash
Boise State University

 DOI: 10.1029/2010WR010367

3-D transient hydraulic tomography in unconfined aquifers with fast drainage response

M. Cardiff[1,2] and W. Barrash[1]

Received 4 January 2011; revised 28 October 2011; accepted 31 October 2011; published 16 December 2011.

[1] We investigate, through numerical experiments, the viability of three-dimensional transient hydraulic tomography (3DTHT) for identifying the spatial distribution of groundwater flow parameters (primarily, hydraulic conductivity K) in permeable, unconfined aquifers. To invert the large amount of transient data collected from 3DTHT surveys, we utilize an iterative geostatistical inversion strategy in which outer iterations progressively increase the number of data points fitted and inner iterations solve the quasi-linear geostatistical formulas of Kitanidis. In order to base our numerical experiments around realistic scenarios, we utilize pumping rates, geometries, and test lengths similar to those attainable during 3DTHT field campaigns performed at the Boise Hydrogeophysical Research Site (BHRS). We also utilize hydrologic parameters that are similar to those observed at the BHRS and in other unconsolidated, unconfined fluvial aquifers. In addition to estimating K, we test the ability of 3DTHT to estimate both average storage values (specific storage S_s and specific yield S_y) as well as spatial variability in storage coefficients. The effects of model conceptualization errors during unconfined 3DTHT are investigated including: (1) assuming constant storage coefficients during inversion and (2) assuming stationary geostatistical parameter variability. Overall, our findings indicate that estimation of K is slightly degraded if storage parameters must be jointly estimated, but that this effect is quite small compared with the degradation of estimates due to violation of "structural" geostatistical assumptions. Practically, we find for our scenarios that assuming constant storage values during inversion does not appear to have a significant effect on K estimates or uncertainty bounds.

Citation: Cardiff, M., and W. Barrash (2011), 3-D transient hydraulic tomography in unconfined aquifers with fast drainage response, *Water Resour. Res.*, *47*, W12518, doi:10.1029/2010WR010367.

1. Introduction

[2] Three-dimensional (3-D) hydraulic tomography (HT) consists of a series of pumping tests in which both pumping and measurement can take place at discrete, isolated depths. By collecting data at a variety of lateral locations and a variety of isolated depths, 3DHT allows for the estimation of 3-D hydraulic parameters (e.g., hydraulic conductivity K, and specific storage S_s). This is in stark contrast to "traditional" pumping tests where water is pumped at an open wellbore and water level changes are measured at surrounding wells, which do not measure vertical variations in head and are thus only capable of estimating depth-integrated or averaged parameters (transmissivity T and storativity S), even if they are analyzed in a tomographic fashion; we will refer to this as 2DHT. Another key differentiator between 3DHT and traditional pumping tests is the time and equipment costs required for 3-DHT surveys in the field. 3DHT with 3-D stimulations of the aquifer requires a method for pumping from a discrete interval either with permanent or temporary installations, for example, packer and port systems that can be moved within an existing wellbore. In addition, either emplaced pressure sensors at depths within the aquifer (e.g., direct push sensors *Butler et al.* [2002]), or hydraulic separation of intervals in existing wellbores (e.g., packer and port systems) must be installed at observation locations in order to obtain information on depth variations of head within the aquifer.

[3] Analyzing pressure response data (i.e., head or changes in head) from pumping tests in a tomographic fashion has been the subject of study for over 15 years, and the literature in this area is extensive. As noted in earlier discussions [*Cardiff*, 2010], approaches to HT "differ in the type of aquifer stimulations they perform (largely 2-D when using fully penetrating wells or 3-D when using packed-off intervals), the type of forward model employed during inversion (2-D, 3-D, axisymmetric 1-D/2-D), the types of heterogeneity assumed (layered 1-D, 2-D cross sectional, 2-D map view, 3-D), constraints on the heterogeneity (geostatistical, structural, or otherwise), and the types of auxiliary data utilized (geophysical, core sample, etc.)." In order to present a perspective about the state of HT research to date, Table 1 is an attempt to summarize and classify the research in 2DHT and 3DHT. In order to limit the size of this table, we consider

[1]Center for Geophysical Investigation of the Shallow Subsurface (CGISS), Department of Geosciences, Boise State University, Boise, Idaho, USA.
[2]Department of Geosciences, University of Wisconsin-Madison, Madison, Wisconsin, USA.

0043-1397/11/2010WR010367

Table 1. Summary of Prior 2DHT and 3DHT Studies

Authors [Year]	Type of Study	Pumping Stimulation Type	Head Response Measurement Type	True Parameter Distribution[a,b,c]	Head Response Data Used[d]	Parameters Estimated[e,f]	Parameter Constraints/ Regularizers/Assumed Prior Information[g]	Other Data Sources Used in Inversion
Gottlieb and Dietrich [1995]	Numerical	2-D, Fully Penetrating *y*	2-D, Fully Penetrating *y*	2-D $K(x,z)$: Facies-Based 0-D Ss: Constant	Transient	2-D $K(x,z)$	$K(x,z)$: zeroth-order Tikhonov Regularization	
Yeh et al. [1996]	Numerical	2-D, Fully Penetrating *z*	2-D, Fully Penetrating *z*	2-D $K(x,y)$: Anisotropic Geostatistical	Steady State	2-D $K(x,y)$	$K(x,y)$: Anisotropic Geostatistical	
Vasco et al. [1997]	Numerical	2-D, Fully Penetrating *y*	2-D, Fully Penetrating *y*	2-D $K(x,z)$: Geostatistical 0-D Ss[h]	Transient, Selected time steps	2-D $K(x,z)$	$K(x,z)$: first-order Tikhonov Regularization	Some analyses of resolution include tracer data
Vasco et al. [1997]	Field	2-D, Fully Penetrating *y*	2-D, Fully Penetrating *y*		Transient, Selected time steps	2-D $K(x,z)$	$K(x,z)$: first-order Tikhonov Regularization	
Snodgrass and Kitanidis [1998]	Numerical	2-D, Fully Penetrating *z*	2-D, Fully Penetrating *z*	2-D $K(x,y)$: Facies-Based	Steady State	2-D $K(x,y)$	$K(x,y)$: Geostatistical[i]	
Zimmerman et al. [1998]	Numerical	2-D, Fully Penetrating *z*	2D, Fully Penetrating *z*	2-D $K(x,y)$: Combined Geostatistical + Facies 0-D Ss	Transient	Variable[j]	Variable[j]	
Zimmerman et al. [1998]	Numerical	2-D, Fully Penetrating *z*	2-D, Fully Penetrating *z*	2-D $K(x,y)$: Combined Geostatistical + Facies 0-D Ss[h]	Transient	Variable[k]	Variable[k]	
Vasco et al. [2000]	Numerical	2-D, Fully Penetrating *z*	2-D, Fully Penetrating *z*	2-D $K(x,y)$: Geostatistical 0-D Ss[h]	Transient, Pulse traveltime metrics	2-D $K(x,y)$	$K(x,y)$: zeroth- and first-order Tikhonov	
Vasco et al. [2000]	Field	2-D, Fully Penetrating *z*	2-D, Fully Penetrating *z*		Transient, Pulse traveltime metrics	2-D $K(x,y)$	$K(x,y)$: zeroth- and first-order Tikhonov	
Yeh and Liu [2000]	Numerical	2-D, Fully Penetrating *z*	2-D, Fully Penetrating *z*	2-D $K(x,y)$: Anisotropic Geostatistical	Steady State	2-D $K(x,y)$	$K(x,y)$: Anisotropic Geostatistical	Point measurements of K (2)
Yeh and Liu [2000]	Numerical	3-D	3-D	3-D $K(x,y,z)$: Anisotropic Geostatistical	Steady State	3-D $K(x,y,z)$	$K(x,y,z)$: Anisotropic Geostatistical	Point measurements of K (2)
Vasco and Karasaki [2001]	Numerical	2-D, Fully Penetrating *y*	2-D, Fully Penetrating *y*	2-D $K(x,z)$: Facies-Based	Transient, Selected time steps	2-D $K(x,z)$	$K(x,z)$: zeroth-order Tikhonov Regularization	
Vasco and Karasaki [2001]	Field	3-D	3-D		Transient, Selected time steps	2-D $K(x,z)$	$K(x,z)$: zeroth- and first-order Tikhonov	
Bohling et al. [2002]	Numerical	3-D[l]	3-D[l]	2-D $K(r,z)$: Anisotropic Geostatistical 0-D Ss: Constant	Transient	1-D $K(z)$ 0-D Ss	$K(z)$: No constraints on *z* variability	
Bohling et al. [2002]	Numerical	3-D[l]	3-D[l]	2-D $K(r,z)$: Anisotropic Geostatistical 0-D Ss: Constant	Transient, Steady Shape	1-D $K(z)$	$K(z)$: No constraints on *z* variability	
Liu et al. [2002]	Laboratory	2-D, Fully Penetrating *y*	2-D, Fully Penetrating *y*	2-D $K(x,z)$: Facies-Based[m] 2-D $Ss(x,z)$: Facies-Based[m]	Steady State	2-D $K(x,z)$	$K(x,z)$: Anisotropic Geostatistical	Point measurement of K (1)
Liu et al. [2002]	Laboratory	2-D, Fully Penetrating *y*	2-D, Fully Penetrating *y*	2-D $K(x,z)$: Facies-Based[m] 2-D $Ss(x,z)$: Facies-Based[m]	Steady State	2-D $K(x,z)$	$K(x,z)$: Anisotropic Geostatistical	Point measurement of K (1)
Liu et al. [2002]	Numerical	2-D, Fully Penetrating *y*	2-D, Fully Penetrating *y*	2-D $K(x,z)$: Facies-Based	Steady State	2-D $K(x,z)$	$K(x,z)$: Anisotropic Geostatistical	Point measurement of K (1)
Liu et al. [2002]	Numerical	2-D, Fully Penetrating *y*	2-D, Fully Penetrating *y*	2-D $K(x,z)$: Facies-Based	Steady State	2-D $K(x,z)$	$K(x,z)$: Anisotropic Geostatistical	Point measurement of K (1)
Vasco and Finsterle [2004]	Field	2-D, Fully Penetrating *y*	2-D, Fully Penetrating *y*		Transient, Pulse traveltime metrics	2-D $K(x,z)$	$K(x,z)$: first-order Tikhonov Regularization	Tracer traveltime metrics
Li et al. [2005]	Numerical	2-D, Fully Penetrating *z*	2-D, Fully Penetrating *z*	2-D $K(x,y)$: Anisotropic Geostatistical 2-D $Ss(x,y)$: Anisotropic Geostatistical	Transient, Moments of drawdown	2-D $K(x,y)$ 2-D $Ss(x,y)$	$K(x,y)$: Geostatistical $Ss(x,y)$: Geostatistic	

Table 1. (continued)

Authors [Year]	Type of Study	Pumping Stimulation Type	Head Response Measurement Type	True Parameter Distribution[a,b,c]	Head Response Data Used[d]	Parameters Estimated[e,f]	Parameter Constraints/ Regularizers/Assumed Prior Information[g]	Other Data Sources Used in Inversion
Li et al. [2005]	Numerical	2-D, Fully Penetrating *z*	2-D, Fully Penetrating *z*	2-D $K(x,y)$: Anisotropic Geostatistical 0-D *Ss*	Transient, Moments of drawdown	2-D $K(x,y)$ 0-D *Ss*	$K(x,y)$: Geostatistical	
Li et al. [2005]	Numerical	2-D, Fully Penetrating *z*	2-D, Fully Penetrating *z*	2-D $K(x,y)$: Anisotropic Geostatistical 0-D *Ss*	Transient, Moments of drawdown	2-D $K(x,y)$ 2-D $Ss(x,y)$	$K(x,y)$: Geostatistical $Ss(x,y)$: Geostatistical	
Li et al. [2005]	Numerical	2-D, Fully Penetrating *z*	2-D, Fully Penetrating *z*	2-D $K(x,y)$: Anisotropic Geostatistical 2-D $Ss(x,y)$: Anisotropic Geostatistical	Transient, Moments of drawdown	2-D $K(x,y)$ 0-D *Ss*	$K(x,y)$: Geostatistical	
Li et al. [2005]	Numerical	2-D, Fully Penetrating *z*	2-D, Fully Penetrating *z*	2-D $K(x,y)$: Anisotropic Geostatistical 2-D $Ss(x,y)$: Anisotropic Geostatistical	Transient, Moments of drawdown	2-D $K(x,y)$ 2-D $Ss(x,y)$	$K(x,y)$: Geostatistical $Ss(x,y)$: Geostatistical	
Zhu and Yeh [2005]	Numerical	1-D, Fully Penetrating *y,z*	1-D, Fully Penetrating *y,z*	1-D $K(x)$: Geostatistical 1-D $Ss(x)$: Geostatistical	Transient, Selected time steps	1-D $K(x)$ 1-D $Ss(x)$	$K(x)$: Geostatistical $Ss(x)$: Geostatistical	Point measurement of K (1) Point measurement of *Ss* (1)
Zhu and Yeh [2005]	Numerical	3-D	3-D	3-D $K(x,y,z)$: Anisotropic Geostatistical 3-D $Ss(x,y,z)$: Anisotropic Geostatistical	Transient, Selected time steps	3-D $K(x,y,z)$ 3-D $Ss(x,y,z)$	$K(x,y,z)$: Anisotropic Geostatistical $Ss(x,y,z)$: Anisotropic Geostatistical	Point measurement of K (1) Point measurement of *Ss* (1)
Vasco and Karasaki [2006]	Numerical	2-D, Fully Penetrating *y*	2-D, Fully Penetrating *y*	2-D $K(x,z)$: Facies-Based 0-D *Ss*	Transient, Pulse traveltime metrics	2-D $K(x,z)$	$K(x,y)$: zeroth- and first-order Tikhonov	
Vasco and Karasaki [2006]	Field	3-D	3-D		Transient, Pulse traveltime metrics	2-D $K(x,z)$	$K(x,z)$: zeroth- and first-order Tikhonov	
Zhu and Yeh [2006]	Numerical	2-D, Fully Penetrating *z*	2-D, Fully Penetrating *z*	2-D $K(x,y)$: Geostatistical 2-D $Ss(x,y)$: Geostatistical	Transient, Selected time steps	2-D $K(x,z)$ 2D $Ss(x,z)$	$K(x,y,z)$: Geostatistical $Ss(x,y,z)$: Geostatistical	
Zhu and Yeh [2006]	Numerical	2-D, Fully Penetrating *z*	2-D, Fully Penetrating *z*	2-D $K(x,y)$: Geostatistical 2-D $Ss(x,y)$: Geostatistical	Transient, Moments of drawdown	2-D $K(x,z)$ 2-D $Ss(x,z)$	$K(x,y,z)$: Geostatistical $Ss(x,y,z)$: Geostatistical	
Zhu and Yeh [2006]	Numerical	2-D, Fully Penetrating *z*	2-D, Fully Penetrating *z*	2-D $K(x,y)$: Geostatistical 2-D $Ss(x,y)$: Geostatistical	Transient, Selected time steps	2-D $K(x,z)$ 2-D $Ss(x,z)$	$K(x,y,z)$: Geostatistical $Ss(x,y,z)$: Geostatistical	
Zhu and Yeh [2006]	Numerical	2-D, Fully Penetrating *z*	2-D, Fully Penetrating *z*	2-D $K(x,y)$: Geostatistical 2-D $Ss(x,y)$: Geostatistical	Transient, Moments of drawdown	2-D $K(x,z)$ 2-D $Ss(x,z)$	$K(x,y,z)$: Geostatistical $Ss(x,y,z)$: Geostatistical	
Bohling et al. [2007]	Field	3-D	3-D		Transient	1-D $K(z)$ 0-D *Ss*	$K(z)$: 1, 5, 7, 10, or 14 Equal-thickness layers.	
Bohling et al. [2007]	Field	3-D	3-D		Transient, Steady Shape	1-D $K(z)$	$K(z)$: 1, 5, 7, 10, or 14 Equal-thickness layers.	
Bohling et al. [2007]	Field	3-D	3-D		Transient, Selected time steps	1-D $K(z)$ 0-D *Ss*	$K(z)$: 5, 7, 10, or 13 Irregular thickness layers	Layer thicknesses informed by zero-offset GPR data
Bohling et al. [2007]	Field	3-D	3-D		Transient, Steady Shape	1-D $K(z)$	$K(z)$: 5, 7, 10, or 13 Irregular thickness layers	Layer thicknesses informed by zero-offset GPR data
Brauchler et al. [2007]	Numerical	3-D[l]	3-D[l]	1-D $K(z)$: Facies-Based 0-D *Ss*	Transient, Pulse traveltime metrics	2-D $D(r,z)$	$D(r,z)$: Coarse, even-determined grid	

Table 1. (continued)

Authors [Year]	Type of Study	Pumping Stimulation Type	Head Response Measurement Type	True Parameter Distribution[a,b,c]	Head Response Data Used[d]	Parameters Estimated[e,f]	Parameter Constraints/ Regularizers/Assumed Prior Information[g]	Other Data Sources Used in Inversion
Brauchler et al. [2007]	Numerical	3-D[l]	3-D[l]	1-D $K(z)$: Facies-Based 0-D Ss	Transient, Pulse traveltime metrics	2-D $D(r,z)$	$D(r,z)$: Coarse, even-determined grid	
Brauchler et al. [2007]	Numerical	3-D[l]	3-D[l]	2-D $K(r,z)$: Facies-Based 0-D Ss	Transient, Pulse traveltime metrics	2-D $D(r,z)$[n]	$D(r,z)$: Coarse, even-determined grid	
Illman et al. [2007]	Numerical	2-D, Fully Penetrating y	2-D, Fully Penetrating y	2-D $K(x,z)$: Facies-Based	Steady State	2-D $K(x,z)$	$K(x,z)$: Anisotropic Geostatistical	Point measurements of K
Illman et al. [2007]	Laboratory	2-D, Fully Penetrating y	2-D, Fully Penetrating y	2-D $K(x,z)$: Facies-Based[m] 2-D $Ss(x,z)$: Facies-Based[m]	Steady State	2-D $K(x,z)$	$K(x,z)$: Anisotropic Geostatistical	
Li et al. [2007]	Field	2-D, Fully Penetrating z	2-D, Fully Penetrating z		Transient, Moments of drawdown	2-D $K(x,y)$ 2-D $Ss(x,y)$	$K(x,y)$: Geostatistical[o] $Ss(x,y)$: Geostatistical[o]	
Li et al. [2007]	Field	2-D, Fully Penetrating z	2-D, Fully Penetrating z		Transient, Moments of drawdown	2-D $K(x,y)$ 0-D Ss	$K(x,y)$: Geostatistical[o]	
Liu et al. [2007]	Laboratory	2-D, Fully Penetrating y	2-D, Fully Penetrating y	2-D $K(x,z)$: Facies-Based[m] 2-D $Ss(x,z)$: Facies-Based[m]	Transient, Selected time steps	2-D $K(x,z)$ 2-D $Ss(x,z)$	$K(x,z)$: Anisotropic Geostatistical $Ss(x,z)$: Anisotropic Geostatistical	Small-scale data (core, slug tests) and layer thicknesses used to estimate variogram variances, correlation lengths
Straface et al. [2007a]	Field	2-D, Fully Penetrating z	2-D, Fully Penetrating z		Transient, Selected time steps	2-D $K(x,y)$ 0-D Ss[h]	$K(x,y)$: Geostatistical	SP data jointly inverted
Straface et al. [2007b]	Field	2-D, Fully Penetrating z	2-D, Fully Penetrating z		Transient, Selected time steps	2-D $K(x,y)$ 2-D $Ss(x,y)$	$K(x,y)$: Geostatistical $Ss(x,y)$: Geostatistical	
Yeh and Zhu [2007]	Numerical	1-D, Fully Penetrating y, z	1-D, Fully Penetrating y, z	1-D $K(x)$: Geostatistical	Steady State	1-D $K(x)$	$K(x)$: Geostatistical	
Yeh and Zhu [2007]	Numerical	2-D, Fully Penetrating y	2-D, Fully Penetrating y	2-D $K(x,y)$: Geostatistical	Steady State	2-D $K(x,z)$	$K(x,z)$: Geostatistical	Conservative and partitioning tracer data sequentially included
Fienen et al. [2008]	Numerical	2-D, Fully Penetrating z	2-D, Fully Penetrating z	2-D $K(x,y)$: Geostatistical	Steady State	2-D $K(x,z)$	$K(x,z)$: Geostatistical[i]	
Fienen et al. [2008]	Numerical	2-D, Fully Penetrating z	2-D, Fully Penetrating z	2-D $K(x,y)$: Facies-Based	Steady State	2-D $K(x,z)$	$K(x,z)$: Geostatistical[i,p]	
Fienen et al. [2008]	Numerical	2-D, Fully Penetrating z	2-D, Fully Penetrating z	2-D $K(x,y)$: Facies-Based	Steady State	2-D $K(x,z)$	$K(x,z)$: Geostatistical[i,p]	
Hao et al. [2008]	Numerical	2-D, Fully Penetrating y	2-D, Fully Penetrating y	2-D $K(x,z)$: Facies-Based 2-D $Ss(x,z)$: Facies-Based	Transient, Selected time steps	2-D $K(x,z)$	$K(x,z)$: Geostatistical	
Hao et al. [2008]	Numerical	2-D, Fully Penetrating y	2-D, Fully Penetrating y	2-D $K(x,z)$: Facies-Based 2-D $Ss(x,z)$: Facies-Based	Transient, Selected time steps	2-D $K(x,z)$ 2-D $Ss(x,z)$	$K(x,z)$: Geostatistical $Ss(x,z)$: Geostatistical	
Hao et al. [2008]	Numerical	2-D, Fully Penetrating y	2-D, Fully Penetrating y	2-D $K(x,z)$: Facies-Based 2-D $Ss(x,z)$: Facies-Based	Transient, Selected time steps	2-D $K(x,z)$ 2-D $Ss(x,z)$	$K(x,z)$: Geostatistical $Ss(x,z)$: Geostatistical	
Hao et al. [2008]	Numerical	2-D, Fully Penetrating y	2-D, Fully Penetrating y	2-D $K(x,z)$: Facies-Based 2-D $Ss(x,z)$: Facies-Based	Transient, Selected time steps	2-D $K(x,z)$ 2-D $Ss(x,z)$	$K(x,z)$: Geostatistical $Ss(x,z)$: Geostatistical	
Illman et al. [2008]	Numerical	2-D, Fully Penetrating y	2-D, Fully Penetrating y	2-D $K(x,z)$: Facies-Based	Steady State	2-D $K(x,z)$	$K(x,z)$: Anisotropic Geostatistical	
Illman et al. [2008]	Numerical	2-D, Fully Penetrating y	2-D, Fully Penetrating y	2-D $K(x,z)$: Facies-Based	Steady State	2-D $K(x,z)$	$K(x,z)$: Anisotropic Geostatistical	Slug test data used for conditioning
Illman et al. [2008]	Numerical	2-D, Fully Penetrating y	2-D, Fully Penetrating y	2-D $K(x,z)$: Facies-Based	Steady State	2-D $K(x,z)$	$K(x,z)$: Anisotropic Geostatistical	Core samples used for conditioning

Table 1. (continued)

Authors [Year]	Type of Study	Pumping Stimulation Type	Head Response Measurement Type	True Parameter Distribution[a,b,c]	Head Response Data Used[d]	Parameters Estimated[e,f]	Parameter Constraints/ Regularizers/Assumed Prior Information[g]	Other Data Sources Used in Inversion
Illman et al. [2008]	Numerical	2-D, Fully Penetrating y	2-D, Fully Penetrating y	2-D $K(x,z)$: Facies-Based	Steady State	2-D $K(x,z)$	$K(x,z)$: Anisotropic Geostatistical	Single-hole tests used for conditioning
Illman et al. [2008]	Laboratory	2-D, Fully Penetrating y	2-D, Fully Penetrating y	2-D $K(x,z)$: Facies-Based[m] 2-D $Ss(x,z)$: Facies-Based[m]	Steady State	2-D $K(x,z)$	$K(x,z)$: Anisotropic Geostatistical	
Illman et al. [2008]	Laboratory	2-D, Fully Penetrating y	2-D, Fully Penetrating y	2-D $K(x,z)$: Facies-Based[m] 2-D $Ss(x,z)$: Facies-Based[m]	Steady State	2-D $K(x,z)$	$K(x,z)$: Anisotropic Geostatistical	Slug test data used for conditioning
Illman et al. [2008]	Laboratory	2-D, Fully Penetrating y	2-D, Fully Penetrating y	2-D $K(x,z)$: Facies-Based[m] 2-D $Ss(x,z)$: Facies-Based[m]	Steady State	2-D $K(x,z)$	$K(x,z)$: Anisotropic Geostatistical	Core samples used for conditioning
Illman et al. [2008]	Laboratory	2-D, Fully Penetrating y	2-D, Fully Penetrating y	2-D $K(x,z)$: Facies-Based[m] 2-D Ss(x,z): Facies-Based[m]	Steady State	2-D $K(x,z)$	$K(x,z)$: Anisotropic Geostatistical	Single-hole tests used for conditioning
Kuhlman et al. [2008]	Numerical	2-D, Fully Penetrating z	2-D, Fully Penetrating z	2-D $K(x,y)$: Geostatistical 2-D $Ss(x,y)$: Geostatistical	Transient	2-D $K(x,z)$	$K(x,y)$: Geostatistical	
Kuhlman et al. [2008]	Numerical	2-D, Fully Penetrating z	2-D, Fully Penetrating z	2-D $K(x,y)$: Geostatistical 2-D $Ss(x,y)$: Geostatistical	Transient	2-D $K(x,z)$	$K(x,y)$: Geostatistical	
Kuhlman et al. [2008]	Numerical	2-D, Fully Penetrating z	2-D, Fully Penetrating z	2-D $K(x,y)$: Geostatistical 2-D $Ss(x,y)$: Geostatistical	Transient	2-D $K(x,z)$	$K(x,y)$: Geostatistical	
Kuhlman et al. [2008]	Numerical	2-D, Fully Penetrating z	2-D, Fully Penetrating z	2-D $K(x,y)$: Geostatistical 2-D $Ss(x,y)$: Geostatistical	Transient	2-D $K(x,z)$	$K(x,y)$: Geostatistical	
Kuhlman et al. [2008]	Numerical	2-D, Fully Penetrating z	2-D, Fully Penetrating z	2-D $K(x,y)$: Geostatistical 2-D $Ss(x,y)$: Geostatistical	Transient	2-D $K(x,z)$	$K(x,y)$: Geostatistical	
Li et al. [2008]	Field	2-D, Fully Penetrating z	2-D, Fully Penetrating z		Steady State	3-D $K(x,y,z)$	$K(x,y,z)$: Geostatistical	
Li et al. [2008]	Field	2-D, Fully Penetrating z	2-D, Fully Penetrating z		Steady State	3-D $K(x,y,z)$	$K(x,y,z)$: Geostatistical	Flowmeter data jointly inverted to add 3-D variability information
Vasco [2008]	Numerical	2-D, Fully Penetrating z	2-D, Fully Penetrating z	2-D $K(x,y)$: Geostatistical 0-D Ss	Transient, Pulse traveltime metrics	2-D $K(x,y)$	$K(x,y)$: zeroth- and first-order Tikhonov	
Vasco [2008]	Field	2-D, Fully Penetrating z	2-D, Fully Penetrating z		Transient, Pulse traveltime metrics	2-D $K(x,y)$ 0-D Ss[h]	$K(x,y)$: zeroth- and first-order Tikhonov	
Bohling [2009]	Field	3-D	3-D		Transient, Selected time steps	2-D $K(r,z)$[q] 2-D $Ss(r,z)$[q]	$K(r,z)$: SVD[r]	
Bohling [2009]	Field	3-D	3-D		Transient, Steady Shape	2-D $K(r,z)$[q]	$K(r,z)$: SVD[r]	
Cardiff et al. [2009]	Numerical	2-D, Fully Penetrating z	2-D, Fully Penetrating z	2-D $K(x,z)$: Geostatistical	Steady State	2-D $K(x,z)$	$K(x,z)$: Geostatistical	
Cardiff et al. [2009]	Field	2-D, Fully Penetrating z	2-D, Fully Penetrating z		Steady State	2-D $K(x,z)$	$K(x,z)$: Geostatistical[i]	
Castagna and Bellin [2009]	Numerical	2-D, Fully Penetrating y	2-D, Fully Penetrating y	2-D $K(x,z)$: Anisotropic Geostatistical	Transient, Pulse traveltime metrics	2-D $D(r,z)$	$D(r,z)$: 14 Pilot Points[m]	Point measurements of K (10)
Castagna and Bellin [2009]	Numerical	2-D, Fully Penetrating y	2-D, Fully Penetrating y	2-D $K(x,z)$: Anisotropic Geostatistical	Transient, Pulse traveltime metrics	2-D $D(r,z)$	$D(r,z)$: 14 Pilot Points[m]	Point measurements of K (10)
Castagna and Bellin [2009]	Numerical	2-D, Fully Penetrating y	2-D, Fully Penetrating y	2-D $K(x,z)$: Anisotropic Geostatistical	Transient, Pulse traveltime metrics	2-D $K(r,z)$ 0-D Ss	$D(r,z)$: 14 Pilot Points[m]	Point measurements of K (10)
Castagna and Bellin [2009]	Numerical	3-D	3-D	3-D $K(x,y,z)$: Anisotropic Geostatistical 0-D Ss	Transient, Pulse traveltime metrics	3-D $K(x,y,z)$ 0-D Ss[h]	$D(r,z)$: 14 Pilot Points[m]	Point measurements of K (10)
Castagna and Bellin [2009]	Numerical	3-D	3-D	3-D $K(x,y,z)$: Anisotropic Geostatistical 0-D Ss	Transient, Pulse traveltime metrics	3-D $K(x,y,z)$ 0-D Ss[h]	$D(r,z)$: 14 Pilot Points[m]	

Table 1. (continued)

Authors [Year]	Type of Study	Pumping Stimulation Type	Head Response Measurement Type	True Parameter Distribution[a,b,c]	Head Response Data Used[d]	Parameters Estimated[e,f]	Parameter Constraints/ Regularizers/Assumed Prior Information[g]	Other Data Sources Used in Inversion
Illman et al. [2009]	Field	3-D	3-D		Transient, Selected time steps	3-D $K(x,y,z)$ 3-D $Ss(x,y,z)$	$K(x,y,z)$: Geostatistical $Ss(x,y,z)$: Geostatistical	
Ni et al. [2009]	Numerical	2-D, Fully Penetrating z	2-D, Fully Penetrating z	2-D $K(x,y)$: Geostatistical	Steady State	2-D $K(x,y)$	$K(x,y)$: Geostatistical	Point measurements of K (27)
Sun et al. [2009]	Numerical	2-D, Fully Penetrating z	2-D, Fully Penetrating z	2-D $K(x,y)$: Facies 0-D Ss	Transient, Selected time steps[h]	2-D $K(x,y)$	$K(x,y)$: Ensemble of multi-point geostatistical images	Point measurements of K (30)
Sun et al. [2009]	Numerical	2-D, Fully Penetrating z	2-D, Fully Penetrating z	2-D $K(x,y)$: Facies 0-D Ss	Transient, Selected time steps[h]	2-D $K(x,y)$	$K(x,y)$: Ensemble of multi-point geostatistical images	Point measurements of K (15)
Sun et al. [2009]	Numerical	2-D, Fully Penetrating z	2-D, Fully Penetrating z	2-D $K(x,y)$: Facies 0-D Ss	Transient, Selected time steps[h]	2-D $K(x,y)$	$K(x,y)$: Ensemble of multi-point geostatistical images	
Xiang et al. [2009]	Numerical	2-D, Fully Penetrating z	2-D, Fully Penetrating z	2-D $K(x,y)$: Geostatistical 2-D $Ss(x,y)$: Geostatistical	Transient, Selected time steps	2-D $K(x,z)$ 2-D $Ss(x,z)$	$K(x,y)$: Anisotropic Geostatistical $Ss(x,y)$: Anisotropic Geostatistical	
Xiang et al. [2009]	Laboratory	2-D, Fully Penetrating y	2-D, Fully Penetrating y	2-D $K(x,z)$: Facies-Based 2-D $Ss(x,z)$: Facies-Based	Transient, Selected time steps	2-D $K(x,z)$ 2-D $Ss(x,z)$	$K(x,z)$: Anisotropic Geostatistical $Ss(x,z)$: Anisotropic Geostatistic	Point measurements of K and Ss
Yin and Illman [2009]	Laboratory	2-D, Fully Penetrating y	2-D, Fully Penetrating y	2-D $K(x,z)$: Facies-Based 2-D $Ss(x,z)$: Facies-Based	Transient, Moments of drawdown	2-D $K(x,z)$ 2-D Ss(x,z)	$K(x,z)$: Anisotropic Geostatistical $Ss(x,z)$: Anisotropic Geostatistical	
Bohling and Butler [2010]	Numerical	2-D, Fully Penetrating z	2-D, Fully Penetrating z	2-D $K(x,y)$: Facies-Based 2-D $Ss(x,y)$: Facies-Based	Transient	2-D $K(x,y)$ 2-D $Ss(x,y)$	$K(x,y)$: 177 Pilot points with regularization $Ss(x,y)$: 177 Pilot points with regularization	
Bohling and Butler [2010]	Numerical	3-D	3-D	3-D $K(x,y,z)$: Geostatistical	Steady State	3-D $K(x,y,z)$	$K(x,y,z)$: Coarsened grid and small degree of zeroth-order Tikhonov toward prior model	
Brauchler et al. [2010]	Field	3-D	3-D		Transient, Pulse traveltime metrics	2-D $D(r,z)$[s]	$D(r,z)$: Coarse, even-determined grid	
Illman et al. [2010a]	Laboratory	2-D, Fully Penetrating y	2-D, Fully Penetrating y	2-D $K(x,z)$: Facies-Based 2-D $Ss(x,z)$: Facies-Based	Steady State	2-D $K(x,z)$	$K(x,z)$: Geostatistical	
Illman et al. [2010b]	Laboratory	2-D, Fully Penetrating y	2-D, Fully Penetrating y	2-D $K(x,z)$: Facies-Based 2-D $Ss(x,z)$: Facies-Based	Steady State	2-D $K(x,z)$	$K(x,z)$: Geostatistical	
Liu and Kitanidis [2011]	Laboratory	2-D, Fully Penetrating y	2-D, Fully Penetrating y	2-D $K(x,z)$: Facies-Based 2-D $Ss(x,z)$: Facies-Based	Steady State	2-D $K(x,z)$	$K(x,z)$: first-order Tikhonov	
Brauchler et al. [2011]	Field	3-D	3-D		Transient, Pulse traveltime metrics	2-D $D(r,z)$ 2-D $Ss(r,z)$	$D(r,z)$: Coarse, even-determined grid $Ss(r,z)$: Coarse, even-determined grid	
Brauchler et al. [2011]	Field	3-D	3-D		Transient, Pulse traveltime metrics	3-D $D(x,y,z)$ 3-D $Ss(x,y,z)$	$D(x,y,z)$: Coarse, even-determined grid $Ss(r,z)$: Coarse, even-determined grid	
Berg and Illman [2011a]	Laboratory	2-D	2-D	2-D $K(x,z)$: Facies-Based 2-D $Ss(x,z)$: Facies-Based	Transient, Selected time steps	2-D $K(x,z)$ 2-D $Ss(x,z)$	$K(x,z)$: Geostatistical $Ss(x,z)$: Geostatistical	

Table 1. (continued)

Authors [Year]	Type of Study	Pumping Stimulation Type	Head Response Measurement Type	True Parameter Distribution[a,b,c]	Head Response Data Used[d]	Parameters Estimated[e,f]	Parameter Constraints/ Regularizers/Assumed Prior Information[g]	Other Data Sources Used in Inversion
Berg and Illman [2011b]	Field	3-D	3-D		Transient, Selected time steps	3-D $K(x,y,z)$ 3-D $Ss(x,y,z)$	$K(x,y,z)$: Geostatistical $Ss(x,y,z)$: Geostatistical	
Huang et al. [2011]	Field	2-D	2-D		Steady State	2-D $K(x,y)$	$K(x,y)$: Geostatistical	

[a]Unless otherwise specified, "Geostatistical" prior information means assuming a second-order stationary random field with all variogram parameters fixed.

[b]With regards to description of the true heterogeneity, "Facies-Based" is used to describe parameter fields where the major component of variability is due to changes in properties at boundaries (e.g., geologic layers). Of course, some variability may also be included within facies [e.g., *Hao et al.*, 2008].

[c]For field experiments, true parameter distributions cannot generally be defined and are thus not populated (though many authors have correlated HT data against existing data).

[d]For head response data used, "Transient" alone refers to a full or nearly full set of transient head measurements (i.e., a drawdown curve), "Selected time steps" refers to a small subset of head measurements selected per transient record, "Moments of drawdown" refers to calculated temporal moments of transient records, and "Pulse traveltime metrics" refers to phase, amplitude, and/or arrival time metrics for pressure pulses.

[e]In many cases of 2-D inversion or 2-D sample problems, the hydrologic parameters were referred to as Transmissivity (T) and Storativity (S). We assume in these cases that the aquifer has uniform thickness b and can thus be written as 2-D K = 2-D T/b, and 2-D Ss = 2-D S/b,

[f]D refers to hydraulic diffusivity, K/Ss.

[g]In this table, zeroth-order Tikhonov regularization refers to regularization that contains a term penalizing distance between parameter estimate s and a starting model. first-order and second-order Tikhonov regularization refers to regularization containing a term that penalizes first-derivative and second-derivative measures of the parameter field using appropriate roughening matrices.

[h]Test problem 4. In this comparison paper, inversion methods varied by contributor.

[i]Variance of variogram estimated as part of inversion.

[j]Test problem 3. In this comparison paper, inversion methods varied by contributor.

[k]Information not found in article.

[l]3-D simulations used a radially symmetric model, effectively only allowing pumping effects and measurement to vary in r and z.

[m]True values unknown in lab experiments, but assumed to follow distribution of sand packing.

[n]Hydraulic diffusivity estimated during inversion, followed by zonation and estimation of constant K and Ss.

[o]Geostatistical variance and correlation length estimated as part of inversion.

[p]Thresholding used to delineate facies after geostatistical inversion.

[q]Heterogeneity in a 2-D (x,z) plane was mapped to (r,z) planes for different tests.

[r]Images of heterogeneity were not produced, but SVD was suggested, which would produce minimum-length solutions (zeroth-order Tikhonov for the limit of 0 data variance).

[s]Four nonjoint 2-D inversions were performed, compared for consistency in 3-D.

only peer-reviewed papers presenting numerical, laboratory, or field experiments in which a series of pumping tests are used to stimulate an aquifer response and in which a number of pressure responses are jointly inverted to produce images of aquifer heterogeneity. Basic characterization approaches such as curve matching for individual pumping or slug interference tests are not listed since they do not jointly fit all data. Likewise, while the governing equations and stimulations are related in ERT, pneumatic, and other tomographic methods, these are not listed since they are not directly controlled by the same physical parameters and have different errors, uncertainties, stimulation magnitudes, and practical implementation constraints. We believe this table captures the range of important research in HT during the past 15 years, and may help to illuminate areas for future advances in HT. While every effort was made to ensure the accuracy and completeness of this table (e.g., by contacting at least one author from each paper in this table), we apologize in advance for any errors or omissions in this summary. Some lessons can be gleaned from the summary of research presented in Table 1, and are discussed below.

[4] In terms of inversion methods used, geostatistically based approaches based on the works of *Yeh et al.* [1995, 1996] or of *Kitanidis and Vomvoris* [1983] and *Kitanidis* [1995] appear to be the most popular by far. This can be attributed to a variety of reasons—including software availability, for example—but one key factor may be the fact that these methods have analytical solutions for linear forward problems (i.e., they consist of linear optimizations) and have generally been shown to perform well for gradient-based optimization in nonlinear problems. In addition, the use of these methods in a Bayesian interpretation allows for calculation of linearized uncertainty metrics for inverted images, including posterior variance estimates and conditional realizations. While research into more computationally complex, novel methods for inversion [e.g., *Caers*, 2003; *Fienen et al.*, 2008; *Cardiff and Kitanidis*, 2009] will always be valuable for providing alternative interpretations when geostatistical assumptions are violated, and for avoiding an inversion "monoculture," the geostatistical approach to the inverse problem appears for the time being to be among the most practical, realistic, and flexible.

[5] While all aquifers are doubtlessly 3-D, the summary of research also suggests that analyzing HT data for 3-D heterogeneity is a daunting challenge, though the computational requirements are more easily met with each passing year. Whether numerical or field studies, only a handful of works have utilized HT data to image 3-D heterogeneity of aquifer hydraulic conductivity [*Yeh and Liu,* 2000; *Zhu and Yeh,* 2005; *Li et al.*, 2008; *Castagna and Bellin,* 2009; *Illman et al.*, 2009; *Bohling and Butler,* 2010; *Brauchler et al.*, 2011; *Berg and Illman,* 2011b]. Of these, only the works of *Zhu and Yeh* [2005], *Illman et al.* [2009], and *Berg and Illman* [2011b] have also sought to image 3-D heterogeneity in aquifer storage parameters. Likewise, as far as we are aware, there are no laboratory studies in which HT data was utilized to image 3-D heterogeneity in aquifer parameters.

[6] The summary also shows how HT applications have matured recently, in the sense of moving from synthetic experiments to actual application. While there are relatively few papers that present tomographic analyses of actual field data from 2DHT or 3DHT data collection campaigns, there has been a marked increase in field applications in the past 5 years. However, there are still relatively few papers in which 3-D aquifer pumping stimulations and 3-D pressure responses have been used as a data source [*Vasco and Karasaki*, 2006; *Bohling et al.*, 2007; *Bohling*, 2009; *Illman et al.*, 2009; *Brauchler et al.*, 2010; *Berg and Illman*, 2011b], and we are aware of only three very recent works in which 3DHT field data was utilized to image full 3-D heterogeneity in aquifer parameters [*Illman et al.*, 2009; *Brauchler et al.*, 2011; *Berg and Illman*, 2011b].

[7] Finally, even though analysis of unconfined aquifers is an important venture (especially for purposes of contaminant transport monitoring and remediation), the HT papers to date have focused on analyzing confined scenarios or ignored changes in aquifer saturated thickness.

[8] As pointed out by *Bohling and Butler* [2010], the field effort associated with installing 3DHT equipment and operating 3DHT tests can be very high, especially if a large number of tests are required and if the tests must be operated for long periods of time (e.g., to approximate steady state). Efforts to employ HT in the field and especially in unconfined aquifers have also had to deal with numerous constraints and "nuisance" effects that are often not considered in numerical experiments, and which may be difficult to analyze with existing theoretical methods. These include, among others, the following:

[9] 1. Inability to obtain high pumping rates due to cavitation concerns.

[10] 2. Surface pump suction limits.

[11] 3. Lowering of the water level in-well below the pumping interval.

[12] 4. Existence of unsteady and difficult to characterize nonpumping stresses such as river stage changes or evapotranspiration, which may make short testing campaigns desirable.

[13] 5. Inability to reach "steady state" in a reasonable amount of time per test.

[14] 6. Changes in saturated thickness in unconfined aquifers due to pumping, and accompanying drawdown curve response.

[15] The purpose of this paper is to present and test an iterative, practical protocol for 3-D transient hydraulic tomography (3DTHT) and to investigate the performance of the method under realistic field constraints encountered in unconfined aquifers. Specifically, the methodology developed and analysis of the synthetic HT results presented in this paper are geared toward application of HT at the Boise Hydrogeophysical Research Site (BHRS), an unconfined, high permeability sand-and-gravel aquifer adjacent to the Boise River that serves as a test bed for hydrologic and geophysical characterization methods [*Barrash and Clemo*, 2002]. The methodology reflects the fact that the nuisance effects listed above (low attainable pumping rates, long times to achieve steady state, etc.) have been encountered during implementation of 3DTHT at the BHRS, and may be common during actual implementation of 3DTHT as a characterization method at similar contaminated sites. While the modeling results in this paper focus on a synthetic case with known heterogeneity, they utilize design parameters and aquifer parameters that are similar to the BHRS instrumentation and aquifer, respectively. In this sense, this paper evaluates the promise of 3DTHT for

application at the BHRS and in similar shallow, unconfined permeable aquifers—an important area for characterization, given the widespread use of shallow, unconfined fluvial aquifers and the relative ease with which these aquifers can be contaminated.

[16] Our synthetic experiments in this paper are the first we are aware of that investigate 3DTHT in an unconfined aquifer. In addition, we have made efforts to incorporate realistic restrictions that have been encountered in 3DTHT investigations at the BHRS in order to provide a realistic assessment of the resolution and uncertainty that can be expected from 3DHT imaging. The restrictions imposed include a lack of "near-field" boundary conditions, restricted pumping rates, and short pumping tests (required to allow sufficient numbers of tests to be carried out in a reasonable period of time). In particular, for realistic field data collection, short pumping tests may be most useful in that they allow greater spatial coverage (due to the ability to perform more testing configurations under set time constraints), and they reduce the likelihood that other natural or anthropogenic stresses will contribute significantly to aquifer response during the pumping test period. Our application is perhaps most similar to the work of *Zhu and Yeh* [2005], the only other published 3DTHT synthetic experiment we are aware of that performed 3-D imaging of both conductivity and storage aquifer parameters. Under the conditions mentioned above, we seek to answer the following questions:

[17] 1. To what extent is aquifer heterogeneity imaging successful when using relatively short, low flow rate tests?

[18] 2. If storage parameters (S_s and S_y) are relatively constant throughout an aquifer, can they be estimated along with 3-D K variations via 3DTHT?

[19] 3. If storage parameters vary throughout an aquifer, can the spatial variability in all three parameters (K, S_s, and S_y) be accurately estimated (in the sense that their estimates are unbiased and uncertainty estimates are approximately correct)?

[20] In addition to simply assessing, under realistic restrictions, the inversion of transient 3DTHT data for estimates of aquifer hydraulic conductivity and storage parameters, we also seek to answer some open questions with regard to conceptual modeling errors when inverting early time 3DTHT data for unconfined scenarios. Specifically:

[21] 1. If storage parameters vary throughout an aquifer, does assuming constant but unknown values during inversion degrade estimates of K?

[22] 2. What errors are introduced by assuming stationary geostatistics when discrete geologic facies (e.g., layering) are the most prominent form of K variability?

[23] While the answers to these questions are no doubt problem dependent to some extent, we believe the sample cases contained in this paper begin to answer these questions. Likewise, in order to allow these questions to be more fully explored, the models utilized in this paper are available on request from the authors. It should be noted at this point that the investigation in this paper focuses on the effects of conceptual modeling errors but assumes that relatively noise-free, high quality data can be obtained. In that sense, the results presented in this paper represent "best case" answers to the questions posed above, and degradation of accuracy with large measurement errors should be expected.

2. Statement of the Problem

[24] The questions discussed above are investigated for a synthetic, heterogeneous unconfined aquifer with relatively high permeability (common for sand-and-gravel systems) and using field-attainable pumping rates and measurement configurations. The basic description of the assumed governing equations for groundwater flow, and the size and discretization of the numerical model, are described below in sections 2.1 and 2.2, respectively. This model is then utilized to analyze transient 3DTHT performance under a number of analysis cases, as discussed in section 4.1.

2.1. Governing Equations and Numerical Model

[25] We consider groundwater flow under saturated but unconfined conditions, in which the water table is represented as a free surface and in which the drainage dealt with at the free surface is fast enough to be considered "instantaneous" for the given testing protocol.

[26] Under these approximations, within the saturated portion of the aquifer, the governing equations for saturated, unconfined groundwater flow with minimal spatial density gradients applies:

$$S_s\frac{\partial h}{\partial t}=\frac{\partial}{\partial x}\left(K\frac{\partial h}{\partial x}\right)+\frac{\partial}{\partial y}\left(K\frac{\partial h}{\partial y}\right)+\frac{\partial}{\partial z}\left(K\frac{\partial h}{\partial z}\right)+w \quad \text{for } 0<z<\xi, \tag{1}$$

where h is hydraulic head [L], S_s is specific storage [$1/L$], K is hydraulic conductivity [L/T], and w represents any sources or sinks of water in terms of volumetric flow rates per unit volume [$[L^3/T]/L^3$], and where $z = 0$ represents the base of the aquifer and $z=\xi$ represents the location of the water table. The coefficients S_s and K are considered variable in space, and the coefficient w may be variable in both space and time. A no-flux boundary condition is assumed at the base of the aquifer, i.e.,

$$\frac{\partial h}{\partial z}=0 \quad \text{for} \quad z=0. \tag{2}$$

At the lateral boundaries of the aquifer (i.e., for x and y locations far from the area being studied) we assume constant-head boundaries, i.e.,

$$h=h_o \quad \text{at} \quad \Gamma_d, \tag{3}$$

where h_o is a constant head value [L] and Γ_d represents the set of constant head (Dirichlet) boundaries. While we have chosen to use constant head boundaries, other boundary conditions may easily be employed. The elevation of the water table ξ is treated as a dependent variable, and is linked to the head distribution in that it is the location where $h = z$ (assuming pressure head is measured as a deviation from atmospheric pressure). Likewise, h and ξ are linked in that a unit drop in ξ over a unit area results in a proportional volumetric input of S_y [$-$] to the saturated zone. To solve the governing equations, we use the popular MODFLOW [*Harbaugh*, 2005] numerical model under conditions where numerical cells of the model are allowed to drain and water table movement is thus tracked.

[27] It should be noted that while, undoubtedly, water table response is dependent on both fast and slow unsaturated

zone drainage, the instantaneous drainage assumption utilized by the standard MODFLOW groundwater flow process (and further discussed by *Harbaugh* [2005]) is a useful and practical approximation for many unconfined aquifers where either one of the two following conditions are met:

[28] The unconfined aquifer is coarse-grained enough that during a head drop/pumping test the full effective porosity is near instantaneously drained (relative to the speed of the head drop); or

[29] A percentage of the unconfined aquifer's effective porosity drains quickly relative to the speed of the head drop/pumping test, and the rest of the effective porosity contributes a negligible flux during the time period of the head drop/pumping test.

[30] That said, while the standard saturated-flow MODFLOW approximations are useful and can result in faster model runtimes, such an approach is expected to be inaccurate for estimating long-term specific yield when delayed drainage in the vadose zone is important and unaccounted for [see, e.g., *Nwankwor et al.*, 1984; *Narasimhan and Zhu*, 1993; *Endres et al.*, 2007; *Tartakovsky and Neuman*, 2007; *Moench*, 2008; *Mishra and Neuman*, 2010, 2011]. In this case of important delayed drainage, short-term pumping tests such as those discussed herein are expected to return low estimates of true aquifer specific yield and may be thought of as an "effective" specific yield, representative of volume balances only at "early times" [*Nwankwor et al.*, 1984], i.e., time scales comparable to the 3DTHT pumping tests. In cases where characterization of true aquifer specific yield is of crucial importance, our approach should not be applied, and a variably saturated flow model should be used, though this is expected to add significant computational effort (due to increased model nonlinearity) and adds the additional need of estimating pressure/saturation and saturation/relative permeability curve parameters, which must also be considered as possibly spatially variable, and whose expected spatial distributions are very poorly understood at this time.

[31] In this work we will study the identifiability of the hydraulic conductivity variability (K), in particular, under this conceptual model. The results obtained thus provide insights into the use of hydraulic tomography in unconfined aquifers where one of the two conditions listed above are met. More broadly though, we expect that the use of such a model may still provide accurate K estimates for aquifers even when delayed drainage shows nonnegligible effects (see, e.g., the parameter estimation results of *Endres et al.* [2007]).

2.2. Synthetic Data Source

[32] We consider short, 30 min HT experiments in a heterogeneous aquifer 60 m × 60 m in lateral extent and 15 m thick with five fully penetrating wells, as shown in Figure 1. The wells are considered to be packed-off so that pressure

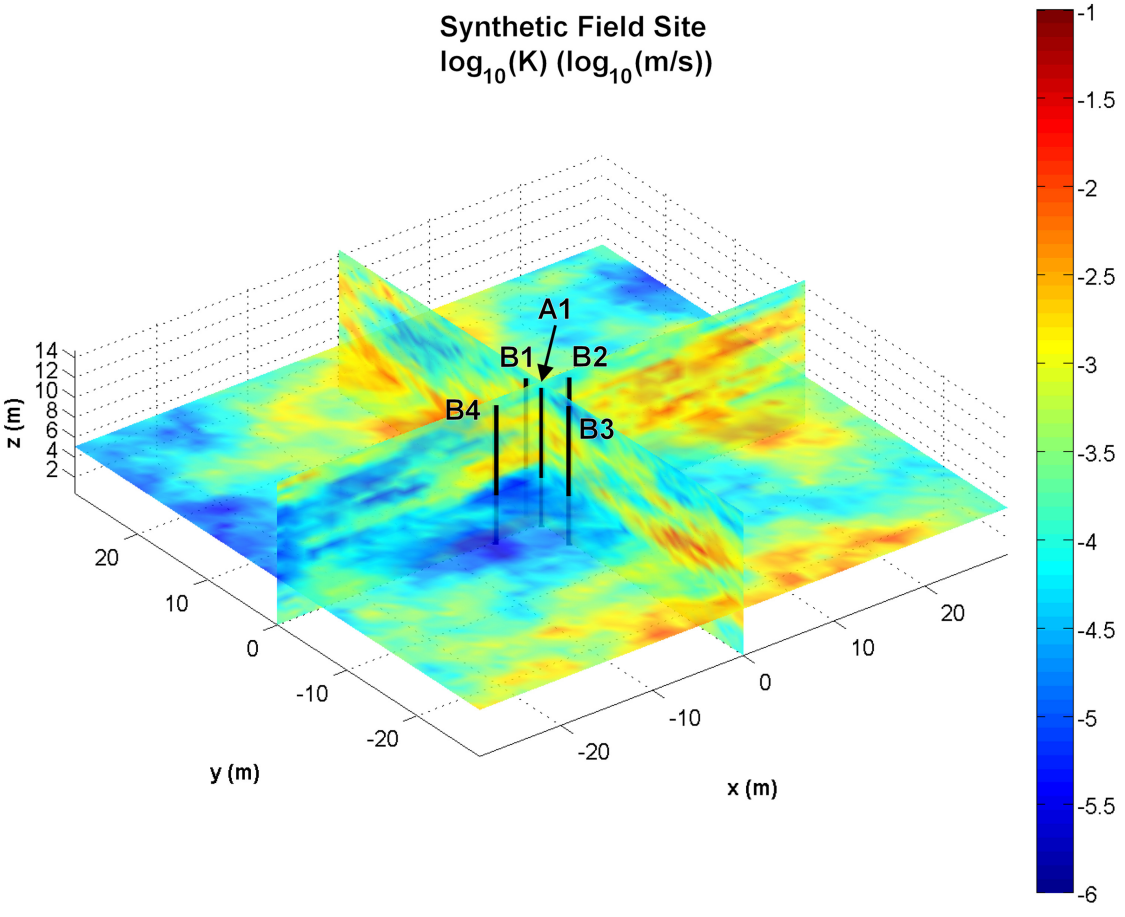

Figure 1. Layout of synthetic field site wells and relative size of modeled domain (60 m × 60 m × 15 m). The slice planes show geostatistically based aquifer K heterogeneity used in analysis cases 1–5.

measurements and pumping can take place at discrete depth intervals. In these tests, pumping at a rate of 0.3 L s^{-1} takes place at the central well (named A1) located at (0 m, 0 m), progressively at elevations of 5, 9, and 12 m. These elevations were chosen in order to produce responses representative of drawdown curves when the pumping interval is far below the water table, at moderate depth, and near the water table, respectively. In the surrounding wells (named B1, B2, B3, and B4 and distanced at 2, 3, 4, and 5 m, respectively) drawdown curves are recorded at four different elevations (4, 7, 10, and 13 m). Pumping is performed at A1 only in order to provide a "baseline" of imaging results when a single well is used for pumping. Rearrangement of pumping and observation instrumentation can require labor-intensive movement of packer and port systems and reassignment of instrumentation to wells. Thus, it is worthwhile to consider the value of a single-well 3DTHT survey when deciding whether the extra effort associated with additional testing arrangements should be carried out for a given aquifer, available testing infrastructure, and problem to be addressed. At the north/south boundaries (positive y/negative y), constant-head values of 14.6 and 14.7 m were applied, respectively, to simulate regional flow across the synthetic site. Constant head boundaries along the east/west (positive x/negative x) were assigned linearly interpolated values between the north and south boundaries. As shown in Figure 1, the pumping and monitored wells are located in the center of the modeling domain and surrounded by a broad heterogeneous extent. This geometry was chosen in order to more realistically represent field uncertainty, where (1) heterogeneity always exists well outside of the given monitoring area, and where (2) near-field constant head or no flux boundaries cannot often be defined. The model geometry and testing strategy are consistent across tests performed in this paper, though different types and amounts of aquifer heterogeneity were examined in the various synthetic tests. While relatively limited in lateral extent compared to real aquifers, the pumping well, operating at a low rate of roughly 5 gpm, and observation wells are both located far from the model boundaries, and analysis of both drawdown and sensitivity matrices indicates that boundary conditions have only minimal effects on the solution. In addition, the short duration of the pumping tests means that the drawdowns do not obtain steady state conditions (see Figure 2). As the data in this figure are plotted in semilog format, it is also apparent that the drawdown does not appear to have clearly attained "steady shape" conditions either [*Jacob*, 1963; *Kruseman and deRidder*, 1990; *Bohling et al.*, 2002].

[33] The aquifer contains heterogeneity in hydraulic conductivity K and, for some analysis cases, heterogeneity in specific storage S_s and specific yield S_y as well. These parameters are discretized on a regular, 1 m × 1 m (laterally) × 0.6 m (thickness) grid, resulting in approximately 90,000 parameter grid cells. We use the same parameter discretization during inversion, meaning each analysis scenario estimates at least 90,000 parameters and in some cases as many as 270,000 (when heterogeneous K, S_s, and S_y are jointly considered).

[34] As discussed above, the aquifer is simulated using the popular and well-tested MODFLOW groundwater flow model [*Harbaugh*, 2005]. In order to improve the accuracy of the simulation, the finite difference grid discretization is further refined relative to the parameter grid (through smaller DELR and DELC spacings) in the vicinity of the pumping and observation wells, resulting in a MODFLOW model with approximately 2 million numerical grid cells. Within the model "natural" steady state head is first attained (assuming no stresses), followed by a 30 min transient stress period in which one of the pumping tests is performed. Using the PCG solver with a tolerance of 0.01 mm required roughly 2–4 min of runtime for a single model run on a single CPU core. Sensitivities of observations to parameter values are calculated using the adjoint-based ADJ process [*Clemo*, 2007], meaning that the number of model runs required for sensitivity matrix evaluation is approximately proportional to the number of observations being inverted.

3. Inverse Solution Method

[35] Synthetic data from the various analysis cases are inverted to produce images of estimated aquifer heterogeneity along with uncertainty estimates (covariance matrices). To efficiently invert these data, we utilize an iterative scheme that progressively includes more data, by fitting more data points on each drawdown curve, as outlined in Figure 3. In what we define as an "outer" iteration, a given set of data is chosen to be inverted, and then supplied to the inner geostatistical inversion loop. The "inner" iterations refer to successive applications of the quasi-linear inversion formulas.

3.1. Outer Iterative Methodology

[36] During each outer iteration in our inverse method, we choose a selection of data points from the full set of recorded field drawdown curves to fit using our forward model. In the first outer iteration, 2–3 or fewer drawdown points may be chosen from each drawdown curve. This may be done either manually or using quantitative metrics (in our case, we have simply selected them manually). These data are inverted (in the inner iteration loop) using the quasi-linear geostatistical inverse method of *Kitanidis* [1995], which inverts all supplied data simultaneously. After inversion of these select data points, a full drawdown curve is generated for each observation location by the forward model and compared to the field data. If each full drawdown curve is not acceptably fit, then another temporal data point is chosen from each field drawdown curve (from a more poorly fit section) and added to the next outer iteration of the inversion (see Figure 3). In each new outer iteration, the best estimate of parameters from the previous outer iteration is utilized as an initial guess in order to speed up convergence. By using fewer data points in early inner iterations, the adjoint state-based sensitivity calculations (whose runtime is proportional to the number of observations, as described below) are less computationally intensive.

[37] In essence, our outer iteration scheme is perhaps most similar to *Li et al.* [2007] in that results from prior iterations are only used to provide initial guesses for parameters during the following iterations. However, we do not utilize moment-based measures of drawdown in our scheme as Li et al. did, instead we simply fit several points on a drawdown curve to match the transient data. One reason we do not use the method of moments is that, because

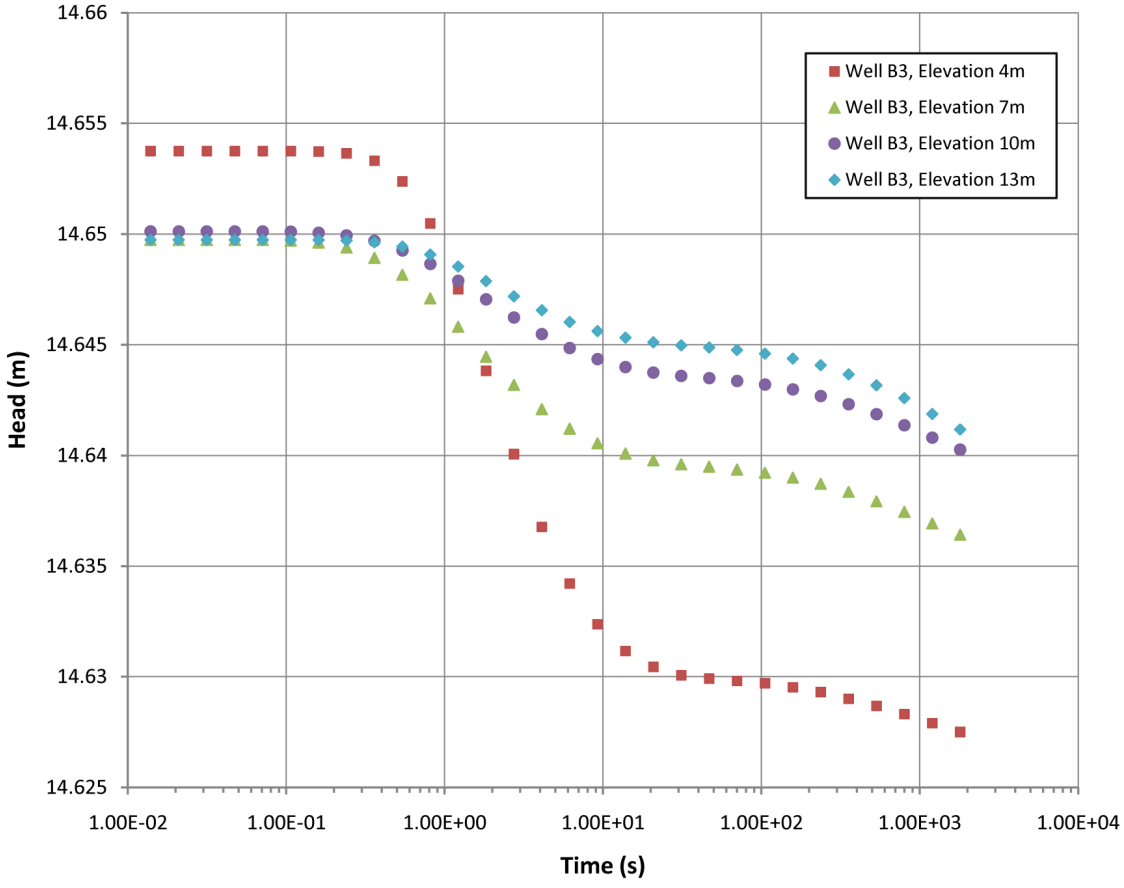

Figure 2. Sample drawdown curves from analysis case 1 for single well and pumping test (test 1, pumping from A1, interval 5 m above datum).

of our unconfined model, we cannot solve for moments of drawdown (at least in the exact sense) using a steady state flow model as Li et al. did. We thus lose the computational advantage of being able to solve a series of steady state flow models instead of full transient models. However, we note that *Yin and Illman* [2009], who fit moments of drawdown during inversion, found their results for estimating storage parameters to be inferior to those of *Liu et al.* [2007], who fit drawdown at selected points in time. It is thus expected that the results obtained using our method will result in more accurate storage parameter estimates than would be obtained by fitting moments of drawdown. Also, the approach of fitting points on the drawdown curve is more generally applicable than the moments-based approach to HT inversion, since in principle it does not need to rely on the required assumptions for generating valid moment-based equations (e.g., that boundary conditions are either constant or no-flux).

3.2. Inner Iteration Inversion System

[38] Within each outer iteration of our inversion, we rely on the quasi-linear geostatistical approach of *Kitanidis and Vomvoris* [1983] and *Kitanidis* [1995], and extensions for large-scale problems based on the work of *Nowak et al.* [2003], to invert the selected data. The basic formulas utilized in this method are summarized below.

[39] Consider that one has measurements available from tests at a field site, as well as a model for simulating these tests with adjustable parameters. The goal, as in all inversion strategies, is to find a set of parameters that fit the data while being "reasonable." In our case, the set of parameters are spatially distributed values of K, as well as possibly S_s and S_y. In the geostatistical approach we perform the minimization

$$\begin{aligned} \min_{\mathbf{s}} L = \min_{\mathbf{s}} \frac{1}{2}[y - \mathbf{h}(\mathbf{s})]^T \mathbf{R}^{-1}[y - \mathbf{h}(\mathbf{s})] \\ + \frac{1}{2}(\mathbf{s} - \mathbf{X}\beta)^T \mathbf{Q}^{-1}(\mathbf{s} - \mathbf{X}\beta), \end{aligned} \tag{4}$$

where $\mathbf{y}$ is an $(n \times 1)$ vector of measured values (the set of all selected data points from all drawdown curves); $\mathbf{h}(\ )$ is a forward model $(\mathbf{R}^m \rightarrow \mathbf{R}^n)$ that takes as input parameter values and outputs expected measurements; $\mathbf{s}$ is a $(m \times 1)$ vector of distributed parameter values; $\mathbf{X}$ is an $(m \times p)$ matrix of drift functions where $\mathbf{X}_{i,j}$ represents drift function j evaluated at the location of parameter $\boldsymbol{s}_i$; β is a $(p \times 1)$ vector of unknown drift coefficients (estimated during inversion); and $\mathbf{R}$ and $\mathbf{Q}$ represent the data error covariance matrix and expected parameter covariance matrix, respectively. Basically, the first term of the minimization seeks to achieve a parameter set that results in a good fit to the

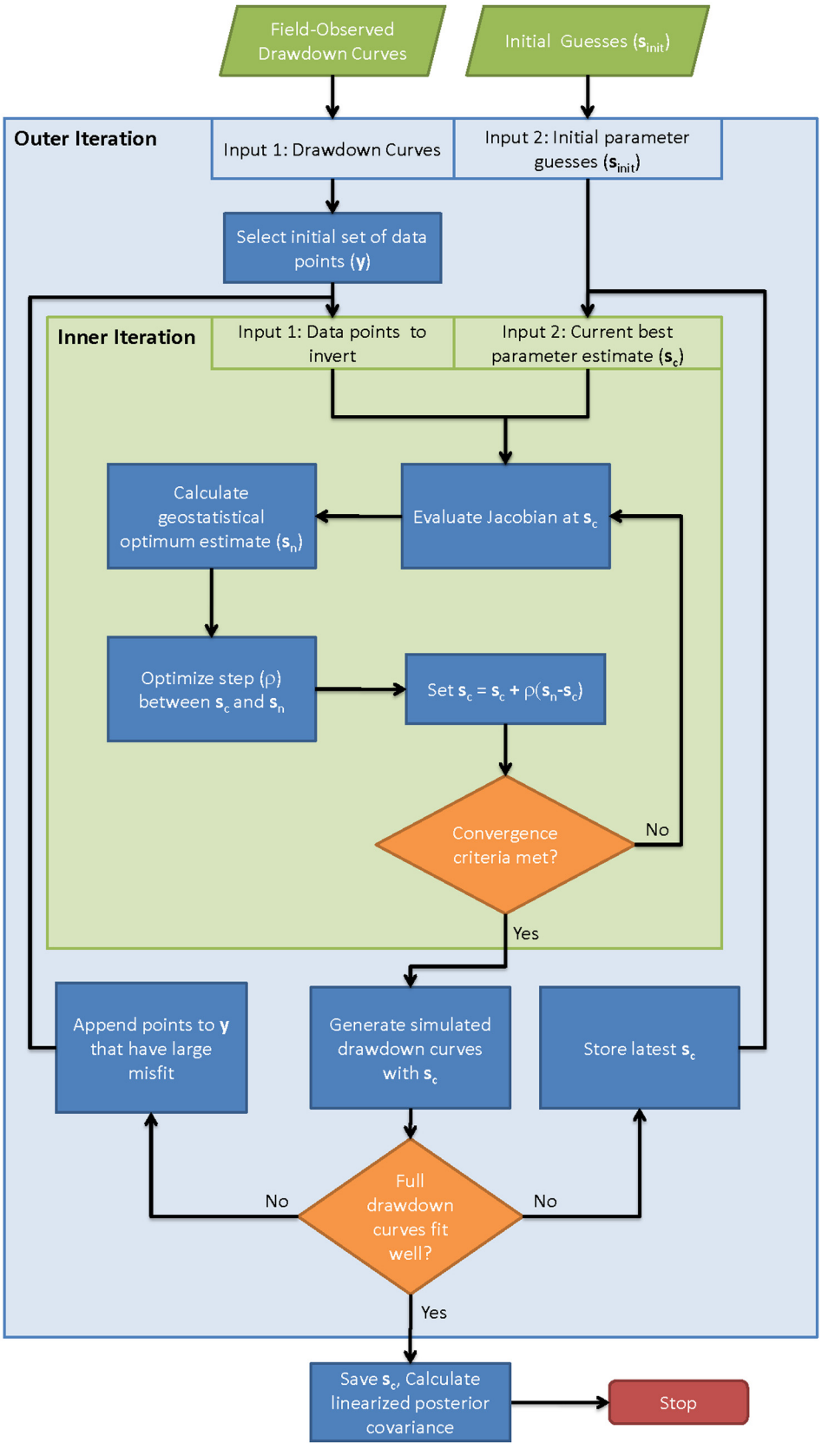

Figure 3. Flowchart for inversion method showing outer iteration loop (observation selection/curve matching) and inner iteration loop (linearization/inversion).

observed data, while the second term seeks to find a parameter set that is "reasonable" given an expected geostatistical distribution. Under the assumption of Gaussian measurement errors (distributed with covariance matrix $\mathbf{R}$) and prior information suggesting a pluri-Gaussian parameter distribution with covariance matrix $\mathbf{Q}$, minimization of $L(\mathbf{s})$ is equivalent to maximizing the posterior probability of the parameter set given the data. It should be noted that, while $\mathbf{R}$ is generally assumed to be a scaled $(n \times n)$ identity matrix (representing independent, identically distributed measurement errors with a given variance), $\mathbf{Q}$ is generally a full $(m \times m)$ matrix with block-Toeplitz structure, assuming the parameter values are being estimated on a regular, equispaced grid. Rather than storing and operating on the full $\mathbf{Q}$ matrix, techniques based on the fast Fourier transform (FFT) are used to calculate matrix-vector multiplications with $\mathbf{Q}$, and can also be used to generate unconditional parameter field realizations with covariance $\mathbf{Q}$ [see *Nowak et al.*, 2003]. These techniques require only storage of the first row of $\mathbf{Q}$, i.e., storage is $O(m)$, and matrix-vector multiplications require computation time proportional to $O[m\log(m)]$ due to the FFT-based methods used.

[40] In the quasi-linear approach to optimizing (4), we assume that we have a current guess at the parameter set, denoted $\mathbf{s}_c$, and we have calculated the expected observations $\mathbf{h}(\mathbf{s}_c)$, for this parameter set. When entering the inner iteration loop, $\mathbf{s}_c$ is set equal to the best parameter estimates from the previous outer iteration; within the inner iteration loop, $\mathbf{s}_c$ is continually updated, as described below. Under a first-order Taylor series expansion, the expected observations at a new parameter set $\mathbf{s}_n$ can be calculated as

$$\mathbf{h}(\mathbf{s}_n) \approx \mathbf{h}(\mathbf{s}_c) + \mathbf{H}_c(\mathbf{s}_n - \mathbf{s}_c), \tag{5}$$

where $\mathbf{H}_c$ is the Jacobian of $\mathbf{h}$ with respect to $\boldsymbol{s}$ evaluated at $\mathbf{s}_c$, i.e., $\mathbf{H}_{c(i,j)} = \frac{\partial \mathbf{h}_i}{\partial \mathbf{s}_j}\big|_{\mathbf{s}_c}$.This means that the value of the objective function L can be approximated as

$$L(\mathbf{s}_n) \approx \frac{1}{2}[\mathbf{y} - \mathbf{h}(\mathbf{s}_c) + \mathbf{H}_c\mathbf{s}_c - \mathbf{H}_c\mathbf{s}_n]^T\mathbf{R}^{-1}[\mathbf{y} - \mathbf{h}(\mathbf{s}_c) + \mathbf{H}_c\mathbf{s}_c - \mathbf{H}_c\mathbf{s}_n] + \frac{1}{2}(\mathbf{s}_n - \mathbf{X}\beta)^T\mathbf{Q}^{-1}(\mathbf{s}_n - \mathbf{X}\beta). \tag{6}$$

Minimizing L with respect to $\mathbf{s}_n$ under this approximation is a quadratic optimization that can be solved in one step by setting the (linear) first derivatives equal to 0. The solution is found by solving the following linear system of equations:

$$\begin{bmatrix} \mathbf{H}_c\mathbf{Q}\mathbf{H}_c^T + \mathbf{R} & \mathbf{H}_c\mathbf{X} \\ (\mathbf{H}_c\mathbf{X})^T & \mathbf{0}_{p\times p} \end{bmatrix} \begin{bmatrix} \xi \\ \beta \end{bmatrix} = \begin{bmatrix} \mathbf{y} - \mathbf{h}(\mathbf{s}_c) + \mathbf{H}_c\mathbf{s}_c \\ \mathbf{0}_{p\times 1} \end{bmatrix}. \tag{7}$$

Once ξ and β are found:

$$\mathbf{s}_n = \mathbf{X}\beta + \mathbf{Q}\mathbf{H}_c^T\xi. \tag{8}$$

In practice, the actual nonlinearity of $\mathbf{h}(\,)$ means that $\mathbf{s}_n$ may not provide the best improvement in the objective function L. A line search is implemented in which the function $L[\mathbf{s}_c + \rho(\mathbf{s}_n - \mathbf{s}_c)]$ is evaluated for several values of the scalar parameter ρ, and the ρ value which produces the minimum L, denoted $\hat{\rho}$, is chosen. Once an optimum $\hat{\rho}$ is found, the problem is linearized around the new best estimate of $\mathbf{s}$, i.e., $\mathbf{s}_c$ is set equal to $\mathbf{s}_c + \hat{\rho}(\mathbf{s}_n - \mathbf{s}_c)$, and the program returns to the beginning of the inner iteration loop. Convergence is declared when either suitably small changes in $\mathbf{s}_c$ between inner iterations are obtained, and/or when small changes in the objective function L between iterations are observed. Once the inner iterations have converged, the program exits the inner iteration loop and returns to the outer iteration loop, where new observations to be fit are selected as necessary.

3.3. Posterior Uncertainty Metrics

[41] Under the Bayesian viewpoint with respect to formula (4), the parameter values found at the end of iteration represent the maximum a posteriori probability (MAP) estimates, i.e., the most likely set of parameter values given the data and prior information. Under first-order probabilistic theory, then, a posteriori estimates of uncertainty in the parameters can also be derived by, basically, taking the inverse of the second derivative (Hessian) of (4) evaluated at the MAP parameter values [e.g., *Kitanidis*, 1996]. A convenient form for the posterior covariance matrix of the parameter estimates, denoted $\mathbf{P}$, is

$$\mathbf{P} = \mathbf{Q} - \begin{bmatrix} \hat{\mathbf{H}}\mathbf{Q} \\ \mathbf{X}^T \end{bmatrix}^T \begin{bmatrix} \hat{\mathbf{H}}\mathbf{Q}\hat{\mathbf{H}}^T + \mathbf{R} & \hat{\mathbf{H}}\mathbf{X} \\ (\hat{\mathbf{H}}\mathbf{X})^T & \mathbf{0} \end{bmatrix}^{-1} \begin{bmatrix} \hat{\mathbf{H}}\mathbf{Q} \\ \mathbf{X}^T \end{bmatrix}, \tag{9}$$

where $\hat{\mathbf{H}}$ represents the sensitivity matrix evaluated at the MAP parameter values $\hat{\mathbf{s}}$. In the case of a linear inverse problem, the posterior covariance matrix obtained via these computations represents the optimal unbiased estimate of the covariance. However, it should be noted that the uncertainty estimate provided by this linearized method in the general case of nonlinear problems is only an approximation of the posterior covariance. Under Cramer-Rao theory, this linearized covariance estimate is generally expected to at least provide a lower bound on the actual, nonlinear covariance.

[42] In general $\mathbf{P}$ is a large, full $(m \times m)$ matrix that is impractical to compute, store, or operate on. For example, in problems such as those investigated in this paper with $O(10^5)$ parameters, double-precision storage of $\mathbf{P}$ would require a minimum of 40 GB, which cannot be operated on in RAM in most modern PCs. In our approach, at the end of the outer iterations, we calculate approximate (linearized) posterior variances for the parameter estimates by only calculating diagonal entries of $\mathbf{P}$ above. While less informative than the full posterior covariance matrix, variances can be used to gauge relative uncertainty in obtained parameter estimates, and to generate approximate conditional realizations in cases where MAP estimates of parameters alone are insufficient (e.g., for follow-on contaminant transport simulation). For example, we suggest the following scheme as a method for generating approximate conditional realizations:

[43] 1. Generate an unconditional realization of $\mathbf{Q}$ using FFT-based methods [*Nowak et al.*, 2003]. Call this realization $\mathbf{s}_u$. Store the square roots of the diagonal elements of $\mathbf{Q}$ (i.e., the prior standard deviations) in a vector σ_{prior}.

[44] 2. Calculate the posterior standard deviations of $\hat{\mathbf{s}}$, the parameter estimates, by evaluating the diagonal elements of $\mathbf{P}$ and taking the square root of each element. Call this vector σ_{post}.

[45] 3. Calculate the approximate conditional realization as $\hat{\mathbf{s}} + (\sigma_{\text{post}}/\sigma_{\text{prior}}) \times \mathbf{s}_u$, where all products and quotients are element wise (i.e., Hadamard products).

[46] Following the steps above will generate a conditional realization that has a mean of $\hat{\mathbf{s}}$, correlation structure based on the variogram used in $\mathbf{Q}$, and variance σ_{post}, i.e., this scheme assumes that while the addition of data has a strong effect on updating the variances of individual parameters, the prior and posterior autocorrelation are not significantly different. In practice, this method can be used to quickly generate candidate parameter fields that are then filtered using acceptance-rejection criteria. The accepted conditional realizations then represent parameter fields that (1) are consistent with the observed 3DTHT data and (2) have realistic geostatistical variability that can be used to more accurately simulate, e.g., plausible contaminant transport scenarios.

4. Application to Synthetic Data

[47] We implement the inversion approach described above for a number of synthetic numerical test cases which differ both in terms of the distribution of storage parameters and in terms of the assumptions utilized during inversion. In all cases except case 5, the K distribution utilized was the same and is as shown in Figure 1.

4.1. Analysis Cases

[48] The basic model setup described above was used to examine several different scenarios and their impact on the performance of 3DTHT for estimation of spatially variable hydraulic conductivity. The analysis cases described below were all carried out on a modern desktop PC (Corei7 processor, 12 GB of RAM) using MODFLOW as the forward model and using a set of MATLAB functions for performing inversion and visualization. Parallelization was implemented in an "embarassingly parallel" fashion, by assigning both forward runs [$\mathbf{h}(\mathbf{s}_c)$ evaluations] and sensitivity calculation ($\mathbf{H}_c$ computations) for individual pumping tests to individual CPU cores. Individual model runs required 2–4 min of CPU time per transient simulation. Sensitivity calculation timings varied with the number of observations inverted during each iteration, but routinely required between 1 and 6 h. In all cases, fewer than 10 sensitivity calculations were required for full convergence (inner and outer iterations). Convergence was declared within inner iterations when either the objective function decrease (change in L) was less than 1% or the maximum relative change in individual $\mathbf{s}_c$ values per iteration was less than 3%. Convergence for the outer iterations was declared when the average misfit of all data points from all drawdown curves was 1 mm or less. As a basis for comparison, the average of the maximum (final) drawdown magnitudes across all measurement locations and all pumping tests was approximately 1.5 cm, meaning we are assuming noise with magnitude of $>7\%$ of the signal. For all cases, we chose one early time, one intermediate-time, and one late-time data point from each drawdown curve to be fit, and found that inclusion of additional data points did not significantly improve data fit.

[49] To assess the accuracy of the computed parameter estimates and their associated uncertainty metrics for each case, we utilized the following measures. First, the root mean square error (RMSE) is used to assess the overall accuracy of the best estimates:

$$\sigma_p = \sqrt{\frac{1}{m}\sum_{i=1}^{m}\left(\mathbf{p}_{\text{true}(i)} - \mathbf{p}_{\text{est}(i)}\right)^2}, \tag{10}$$

where $\mathbf{p}_{\text{true}(i)}$ and $\mathbf{p}_{\text{est}(i)}$ are the true and estimated parameter values [i.e., $\log_{10}(K)$, $\log_{10}(S_s)$, or $\log_{10}(S_y)$] for grid cell i. As an approximate measure of the accuracy of the posterior uncertainty estimates, we similarly calculate the normalized root mean square error (NRMSE) as

$$\nu_p = \sqrt{\frac{1}{m}\sum_{i=1}^{m}\frac{\left(\mathbf{p}_{\text{true}(i)} - \mathbf{p}_{\text{est}(i)}\right)^2}{\mathbf{P}_{(i,i)}}}. \tag{11}$$

In the ideal case where posterior variances are accurate, the NRMSE computed should be close to 1. Since our pumping tests and measurements are focused in a small area relative to the overall model, we calculate these metrics for the entire model but also for the "central area" of our model, which we define as a 10 m $\times$ 10 m $\times$ 15 m prism centered at the x, y coordinates $(0, 0)$. Similarly, since data from these pumping tests are only dependent on S_y values toward the top of our model, we calculate RMSE and NRMSE statistics for S_y for the top-most layer of our model as well as for the overall model.

4.2. Analysis Case 1

[50] In analysis case 1 we assume very strong prior information in the form of perfect knowledge of the storage coefficients. Likewise, the storage coefficients are spatially uniform within the true model. Case 1 represents a baseline analysis case in that estimating K is aided by perfect knowledge of storage coefficients, and in which the lack of storage coefficient variability will eliminate the problem of K/storage coefficient "aliasing" [see, e.g., *Li et al.*, 2005]. In case 1, the only parameters to be estimated are the heterogeneous values of K throughout the model. S_s and S_y values are constant throughout the domain in the true parameter field, and their values are assumed known during inversion. The true $\log_{10}(K)$ field for case 1 is shown in Figure 1, and the geostatistical parameters of the true field are given in Table 2. Note that the relatively low S_y used in all cases is consistent with drainage response at short times, see, e.g., *Neuman* [1975] and *Moench* [1994]. The geostatistical parameters utilized during inversion are the same as those used to generate the heterogeneous parameter field (see Table 3). However, note that the variance of the realization generated and used as the true parameter field (0.41), differs from the model value (0.5) which was used as input to the generation process and was also assumed in the inversion process.

[51] The progressive improvement of data fit during outer iterations is shown in Figure 4. A comparison of the imaging results for case 1 during outer iterations is shown

Table 2. Summary Statistics for True Parameter Fields Used in All Analysis Cases[a]

		Analysis Case		
		1, 2	3, 4	5
$\log_{10}(K)$	Generation Mean ($\log_{10}$(m s^{-1}))	−4	−4	N/A
	Generation Variance ($\log_{10}$(m s^{-1}))^2	0.5	0.5	N/A
	Generation x Correlation Length (m)	15	15	N/A
	Generation y Correlation Length (m)	12	12	N/A
	Generation z Correlation Length (m)	3	3	N/A
	Parameter Field Mean ($\log_{10}$(m s^{-1}))	−3.7	−3.7	−3.6
	Parameter Field Variance ($\log_{10}$(m s^{-1}))	0.41	0.41	1.2
	Minimum Value ($\log_{10}$(m s^{-1}))	−6.22	−6.22	−4.5
	Maximum Value ($\log_{10}$(m s^{-1}))	−1.28	−1.28	−2
$\log_{10}(S_s)$	Generation Mean ($\log_{10}$(1 m^{-1}))	−4.7	−5	N/A
	Generation Variance ($\log_{10}$(1 m^{-1}))^2	N/A	0.08	N/A
	x Correlation Length (m)	N/A	15	N/A
	y Correlation Length (m)	N/A	12	N/A
	z Correlation Length (m)	N/A	3	N/A
	Parameter Field Mean ($\log_{10}$(1 m^{-1}))	−4.7	−4.9	−5.1
	Parameter Field Variance ($\log_{10}$(1 m^{-1}))	N/A	0.066	0.6
	Minimum Value ($\log_{10}$(1 m^{-1}))	N/A	−5.88	−6
	Maximum Value ($\log_{10}$(1 m^{-1}))	N/A	−3.91	−4
$\log_{10}(S_y)$	Generation Mean (−)	−1.6	−1.5	N/A
	Generation Variance (−)	N/A	0.02	N/A
	x Correlation Length (m)	N/A	15	N/A
	y Correlation Length (m)	N/A	12	N/A
	z Correlation Length (m)	N/A	3	N/A
	Parameter Field Mean (−)	−1.6	−1.4	−1.6
	Parameter Field Variance (−)	N/A	0.016	0.15
	Minimum Value (−)	N/A	−1.94	−2
	Maximum Value (−)	N/A	−0.96	−1

[a]For cases where true parameter field was generated from geostatistical models, generation parameters are given.

Table 3. Geostatistical Structural Parameters Assumed During Inversion of All Analysis Cases

		Analysis Case	
		1, 2, 3	4, 5
$\log_{10}(K)$	Assumed Variance ($\log_{10}$(m s^{-1}))^2	0.5	0.5
	Assumed x Correlation Length (m)	15	15
	Assumed y Correlation Length (m)	12	12
	Assumed z Correlation Length (m)	3	3
$\log_{10}(S_s)$	Assumed Variance ($\log_{10}$(1 m^{-1}))^2	N/A	0.08
	Assumed x Correlation Length (m)	N/A	15
	Assumed y Correlation Length (m)	N/A	12
	Assumed z Correlation Length (m)	N/A	3
$\log_{10}(S_y)$	Assumed Variance ($\log_{10}$(1 m^{-1}))^2	N/A	0.02
	Assumed x Correlation Length (m)	N/A	15
	Assumed y Correlation Length (m)	N/A	12
	Assumed z Correlation Length (m)	N/A	3

in Figure 5, which displays both the "best estimate" of parameter values throughout the domain as well as the estimated posterior standard deviation of this estimate, and Figure 6, which shows three slice views comparing the estimates obtained (from two different outer iterations) to the true parameter field within the central area. The general trend visible is that: (1) Slight image improvement is seen as more observations are included in the inversion from the intermediate and early time portion of the drawdown curve; and (2) detailed heterogeneity in the best estimates and relatively low uncertainties are obtained near the pumping and observation locations, while far from the observation locations the best estimates trend toward a uniform, homogeneous value.

[52] The data fit metrics for analysis case 1 are shown in Table 4. Overall we see that RMSE of $\log_{10}(K)$ estimates is much lower in the central area when compared to the full model domain. The NRMSE, which should generally be close to 1, shows that variances for $\log_{10}(K)$ appear to be generally accurate, but are somewhat underestimated within the central area (leading to a NRMSE greater than 1). We believe this effect is due to the fact that our the model sensitivity is more nonlinear due to higher head gradients in this area, meaning that the linearized uncertainty bounds estimated are more inaccurate.

4.3. Example of Approximate Conditional Realization Strategy

[53] While the best estimates obtained by our inversion methodology outside of the central region could be classified as not "geologically realistic" (see, e.g., Figure 5), they reflect our lack of knowledge about heterogeneous structures in this area. As noted by *Bohling and Butler* [2010], there are generally a large number of parameter fields that can be found that are consistent with data collected from HT surveys, especially in cases where significant heterogeneity exists outside the region of the aquifer being interrogated. The best estimates obtained by the geostatistical method, however, represent average features across all possible data-consistent realizations, or at least the best approximation of these average features using linearized theory. The lack of detail in these areas, and accompanying large uncertainty estimates, can provide guides for future data collection during iterative characterization.

[54] In Figure 7 we present a conditional realization generated for case 1 using our proposed approximate strategy, which was selected (filtered) from a group of approximate conditional realizations by the simple technique of "fitting within tolerance" of 1 mm, i.e., the average residuals between observed data and simulated data from the conditional realization was required to be <1 mm. As a basis for comparison to this level of misfit, average residuals obtained when using a fitted homogeneous K model were 6.7 mm.

4.4. Analysis Case 2

[55] The same "true" model featuring spatially variable K but uniform S_s and S_y values was used in case 2, with the key difference being that the homogeneous values of S_s and S_y are estimated in case 2. For this sample case, we found that both S_s and S_y parameters were estimated fairly accurately, the RMSEs presented in Table 4 correspond to a 4% and 40% error in S_s and S_y, respectively. With respect to estimation of K, the inclusion of estimation of unknown homogeneous values of S_s and S_y does not appear to have a

Figure 4. Improvement of drawdown curve fits with successive inclusion of more inverted data points (outer iteration steps). Main image shows example drawdown curve fits for a single well and test (well B3, all elevations, test 1 pumping at A1, 5 m above datum). Inset images show crossplot of all observed versus simulated data at given iteration.

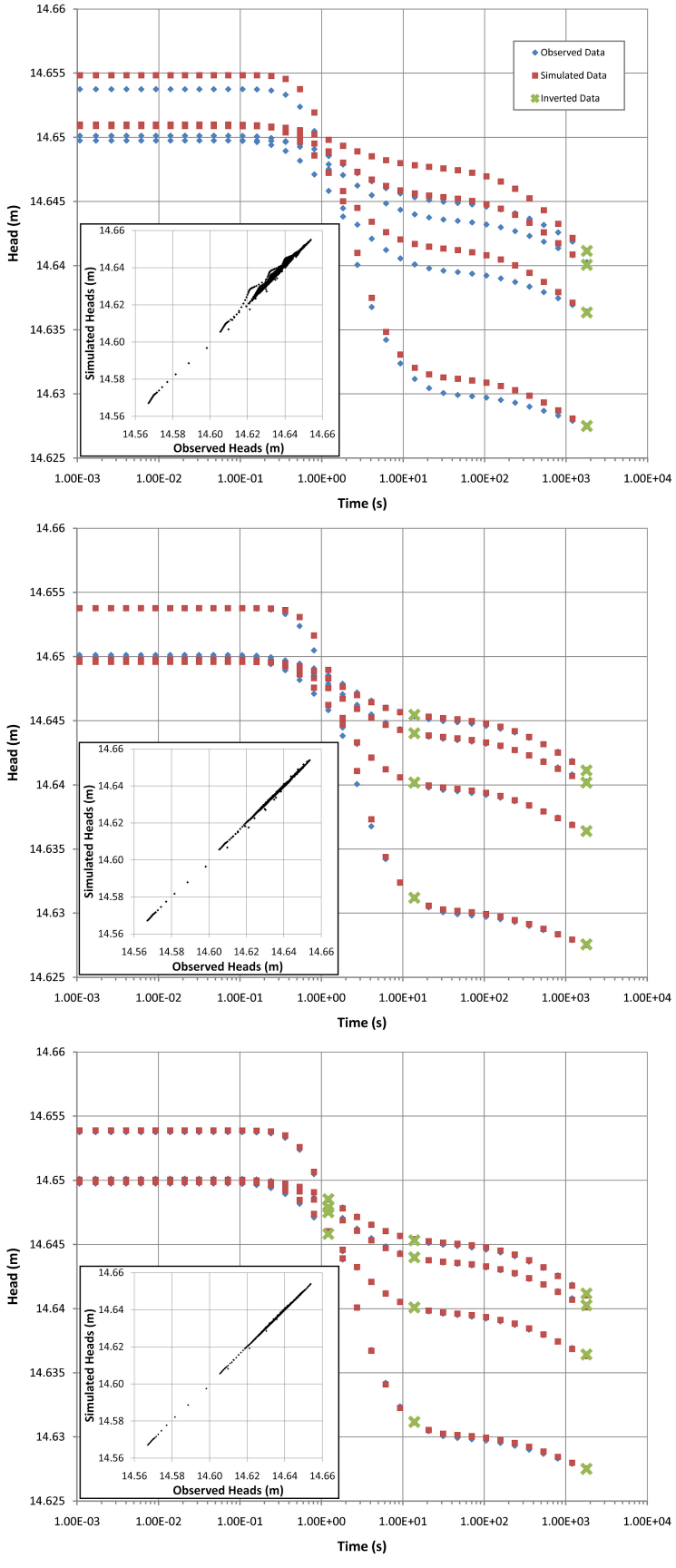
Observed Data
Simulated Data
Inverted Data
Head (m)
Time (s)
Simulated Heads (m)
Observed Heads (m)
14.66
14.655
14.65
14.645
14.64
14.635
14.63
14.625
1.00E-03
1.00E-02
1.00E-01
1.00E+00
1.00E+01
1.00E+02
1.00E+03
1.00E+04
14.56
14.58
14.60
14.62
14.64
14.66

Figure 4

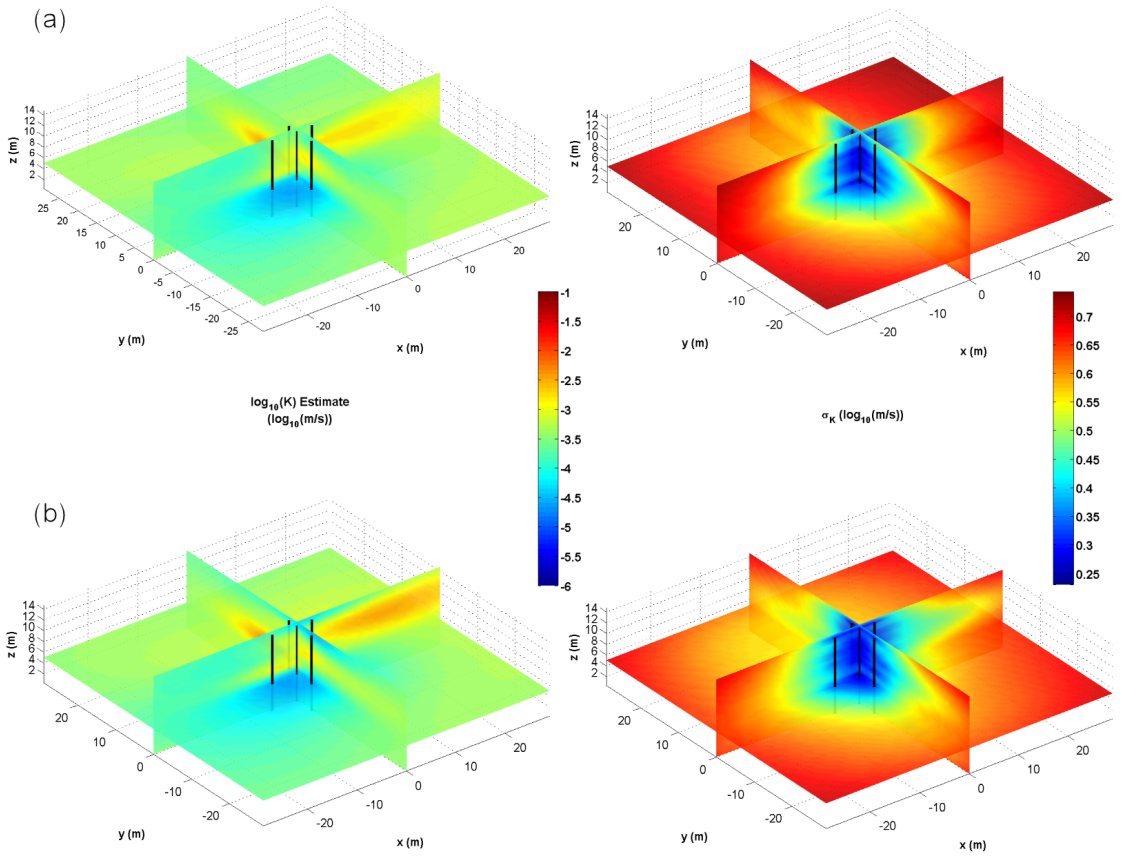

Figure 5. Changes in inverted image and uncertainty estimates progressive inclusion of more data through outer iterations (case 1). Images represent (a) outer iteration 1 and (b) outer iteration 3. Left-hand side images represent best estimates, and right-hand side images represent posterior standard deviation estimates.

major effect on K estimate accuracy, though a small increase in K RMSE is seen in the central area.

4.5. Analysis Case 3

[56] In case 3 we investigate an aquifer with heterogeneous storage coefficients as well as heterogeneous K values. In our particular case, we assume for the true field S_s and S_y values that are correlated with K variability, but with different means and variances than the K field. As discussed by *Li et al.* [2005], there is little information available in the literature about the geostatistical distribution of storage parameters, and their correlation with hydraulic conductivity, for real aquifers. For our sample case, we assume that K, S_s, and S_y are exactly correlated but have different means and variances. This is analogous to assuming a porosity-controlled system where less consolidated, higher porosity units will generally have higher K, higher S_s, and higher S_y values. It should be noted though that this behavior should not always be expected in all conditions. For example, *Straface et al.* [2007b] found during his analysis that transmissivity and storativity parameters did not appear to be correlated at the Montalto Uffugo Scalo field site in Italy. Similarly, *Brauchler et al.* [2010] found anticorrelation between K and S_s at the Stegemühle test site.

[57] The K field in case 3 is the same as the K field in cases 1 and 2. During inversion for case 3, we assume that only K is spatially variable and estimate homogeneous values for both S_s and S_y. K field estimates for this analysis case are slightly worse than those from case 2, in terms of RMSE. Likewise, larger NRMSE values for K in case 3 as compared to case 2 seems to indicate a small degree of aliasing [see, e.g., *Li et al.*, 2005] due to incorrectly assuming constant storage values. The storage coefficients estimated during inversion appear to be close to the geometric mean of the true, heterogeneous parameter field. For S_s the geometric mean of the true parameter field is 1.3×10^{-5} m^{-1}, and the estimated homogeneous value was 8.1×10^{-6} m^{-1}. For S_y, the geometric mean of the true parameter field is 0.037 and the estimated homogeneous value was 0.045.

4.6. Analysis Case 4

[58] In case 4 we seek to jointly estimate the spatial variability in all three parameters (K, S_s, and S_y). We assume during inversion that K, S_s, and S_y variability is *uncorrelated* (even though, in the true field, the parameters are correlated) in order to test the ability of inversion to independently identify these parameters' variability given the data. The true parameter fields used in case 4 are exactly the same as those used in case 3.

[59] In comparison to case 3, we see only very slight changes in the RMSE of the K estimates, suggesting that assuming homogeneous S_s and S_y was not detrimental for

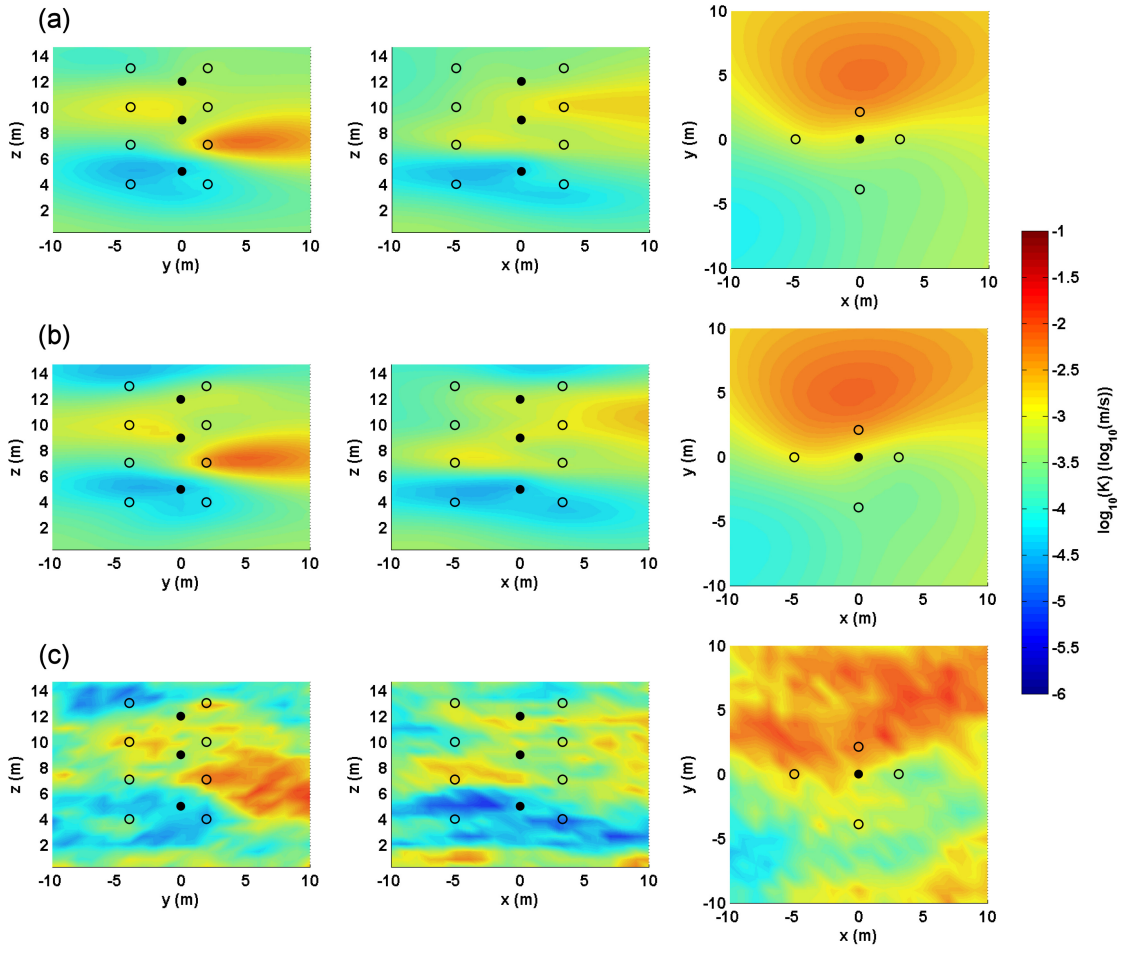

Figure 6. Comparison of best estimates obtained at (a) outer iteration 1 and (b) outer iteration 3 against (c) true parameter field. Images show parameter estimates in central 10 m × 10 m × 15 m area along the slices (from left to right, respectively) $x = 0$ m, $y = 0$ m, and $z = 7.5$ m. Filled dots represent pumping locations and open dots represent observations.

the example considered. In terms of storage estimates, RMSE for S_s and S_y are somewhat smaller than the RMSE for case 3, suggesting that 3DTHT does have some ability to estimate heterogeneity in these parameters. However, the uncertainty estimates obtained by the geostatistical methods for both S_s and S_y appear to be highly inaccurate, as shown by NRMSE values for these parameters that are far from the expected value of unity (Table 4).

Table 4. Fit Statistics Calculated for All Analysis Cases

		Analysis Case				
		1	2	3	4	5
$\log_{10}(K)$ ($\log_{10}$(m s^{-1}))	RMSE	0.572	0.571	0.571	0.571	0.935
	NRMSE	0.959	0.941	0.942	0.930	1.525
	RMSE (central area)	0.360	0.362	0.365	0.366	0.606
	NRMSE (central area)	1.048	1.018	1.021	1.003	1.668
$\log_{10}(S_s)$ ($\log_{10}$(1 m^{-1}))	RMSE	N/A	0.016	0.256	0.255	0.776
	NRMSE	N/A	0.214	2.824	1.804	5.488
	RMSE (central area)	N/A	0.016	0.261	0.240	0.699
	NRMSE (central area)	N/A	0.214	2.876	1.697	4.941
$\log_{10}(S_y)$ (−)	RMSE	N/A	0.140	0.128	0.125	0.389
	NRMSE	N/A	0.994	1.195	0.443	1.377
	RMSE (top layer)	N/A	0.140	0.107	0.104	0.038
	NRMSE (top layer)	N/A	0.994	0.999	0.368	0.134
Full Drawdown Curve Head Values (m)	RMSE	2.30E-04	2.70E-04	1.00E-03	7.90E-04	1.00E-03

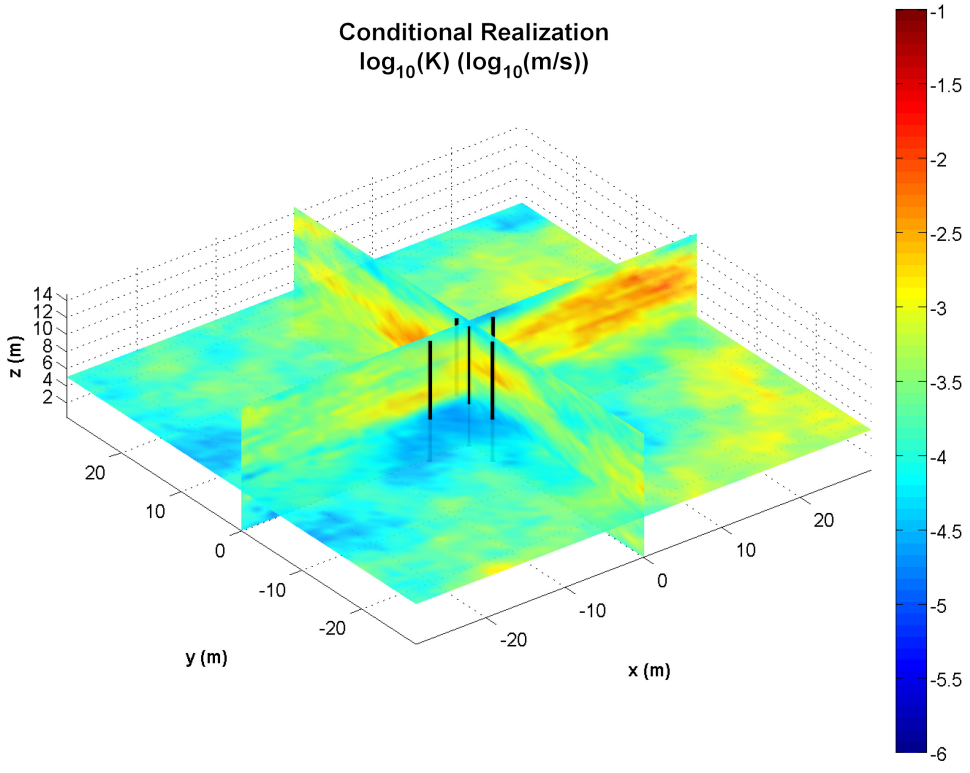

Figure 7. Conditional realization of $\log_{10}(K)$ generated using suggested approximate method. Average data misfit for this realization is 0.6 mm.

4.7. Analysis Case 5

[60] In case 5 we investigate the effect of the model conceptualization error associated with assuming an incorrect (stationary) geostatistical model. The true $\log_{10}(K)$ field for case 5 is different from all other cases, and is shown in Figure 8. The discrete geologic layers in case 5 each have a different, homogeneous value for all three parameters K, S_s, and S_y, as given in Table 5. Overall statistics for this parameter field are given in the last column of Table 2.

[61] During inversion, we incorrectly assume the same geostatistical model as used in case 4. Most significantly, the variance of $\log_{10}(K)$ compared with the true statistics for the facies-based parameter field is underestimated by a factor of 2.4, and the variances of $\log_{10}(S_s)$ and $\log_{10}(S_y)$ are both underestimated by a factor of 7.5. (Note, however, that the minimum and maximum values for all parameters are similar to the values from case 4, see Table 2). These biases reflect the fact that, in field practice, prior estimates of parameter field variances obtained via simple methods—e.g., kriging of pseudo-locally obtained "homogeneous" values—may generally underestimate parameter variability (see, e.g., comparisons by *Li et al.*, [2007]). In addition, these biases reflect the fact that stationary geostatistical models may be assumed when true parameter variability contains nonstationary features.

[62] Graphically, estimates of K within the central area appear fairly accurate (see Figure 8), even though an incorrect geostatistical model has been assumed, but large-scale trends outside of the central well area are poorly represented. Comparison between analysis cases 3 and 5 allows us to investigate the relative errors associated with incorrectly assuming constant storage coefficients (case 3) versus correctly assuming spatial variability in storage coefficients but incorrectly estimating the geostatistical model (case 5). We find that the errors in estimation of K associated with geostatistical model errors are much greater, for our sample cases, than errors associated with assuming constant storage coefficients. Large increases in K RMSE are seen in case 5 relative to case 4, and likewise the NRMSE for K, S_s, and S_y reflect the fact that posterior variances are quite poorly estimated in this sample case.

5. Discussion and Conclusions

[63] We have presented and implemented a geostatistically based inversion strategy for analyzing data from 3DTHT in unconfined aquifers that is able to invert short-term pumping tests where even steady-shape conditions may not be satisfied. Likewise, our inversion strategy does not require constant pumping rates and could be used in scenarios where nonpumping stresses also affect the aquifer throughout the duration of the test. To the best of our knowledge, this work represents the first implementation of 3DTHT data inversion for unconfined aquifers. The general methodology is flexible for implementation in confined scenarios as well, though.

[64] The suggested strategy was tested on a number of sample cases of varying complexity. For all cases, the pumping rates and geometry utilized were based on experience implementing 3DTHT at a well-studied, unconsolidated

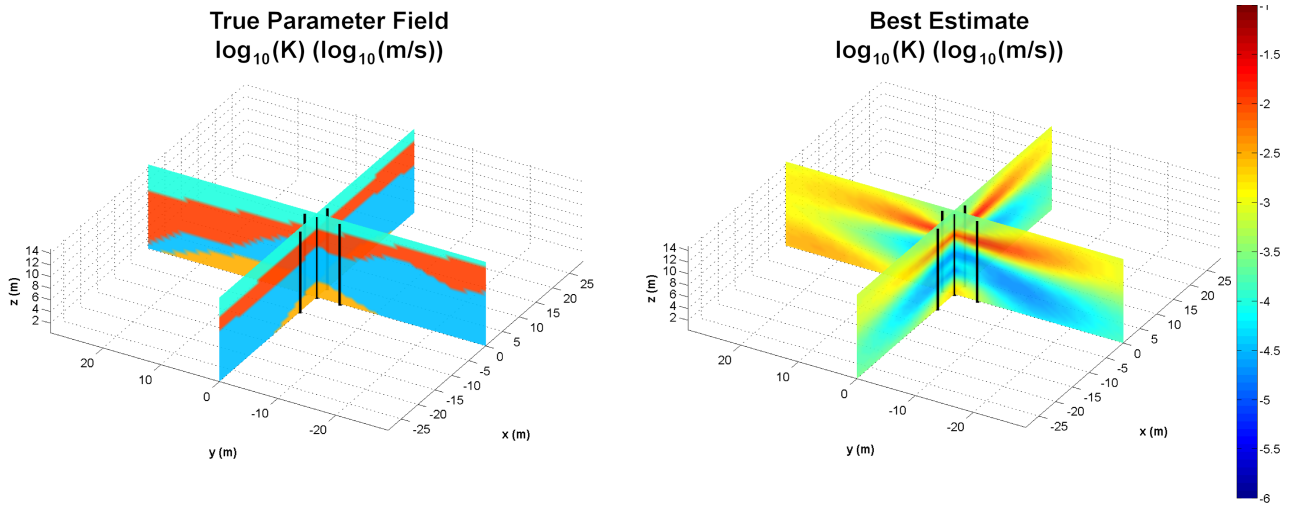

Figure 8. Comparison between true and inverted $\log_{10}(K)$ distribution for case 5, in which the true parameter field consists of distinct layers. Overall accurate images are obtained in vicinity of wells, with increasing error at far distances.

unconfined aquifer, the Boise Hydrogeophysical Research Site. Likewise, the heterogeneity models utilized are presumed to be realistic for the BHRS and other similar unconfined fluvial aquifers. It should be noted that in the examined example, the aquifer being studied has relatively high hydraulic conductivity and (if it were confined) high hydraulic diffusivity. A relatively low pumping rate was utilized which was consistent with obtainable pumping rates during field experimentation. Furthermore, we have made an effort to make our study realistic by assuming a broad aerial extent of heterogeneous aquifer surrounding our well field. All of these factors cause increased difficulty in imaging hydrologic parameters with HT, but may be common in actual application to unconfined, fluvial aquifers.

[65] Several cases were examined in our synthetic experiments. In the case where K is heterogeneous but storage coefficients are reasonably homogeneous within the aquifer being investigated, we find that both S_s and S_y parameters can be estimated with reasonable accuracy (case 2). If S_s and S_y are variable, treating them as homogeneous during inversion appears to result in estimates that are close to the geometric mean of the true storage parameter fields (case 3). If S_s and S_y are variable and treated as variable during inversion (case 4), we find that slight improvement in the parameter estimates can be obtained for the sample case investigated, but that posterior uncertainty estimates for storage coefficients appear to be quite inaccurate, even when correct geostatistics are assumed. Finally, we find that the assumed geostatistical model used during inversion appears to have a much greater influence on the accuracy of K estimates and their associated uncertainty measures than does treating S_s and S_y as constant values (case 5). While not examined here, a possible area for future research is determining the extent to which unconfined conditions will affect inversion results if a confined model is assumed during analysis.

[66] In practice we believe that estimation of K heterogeneity in permeable unconfined aquifers is minimally impacted by assumptions of constant storage coefficients, when considered relative to other sources of error such as inappropriate use of a stationary geostatistical model, mis-estimation of parameter field variances, and mis-estimation of parameter field correlation lengths. Likewise, given that so little information exists in the literature about the range of variability of storage coefficients (particularly S_s) in natural aquifers—and about their correlation or lack thereof with K variability—treating S_s and S_y as constant but unknown parameters during inversion seems to be a practical and computationally efficient approach for estimating K fields in unconfined aquifers. This agrees with the results of *Li et al.* [2005], who found for 2-D confined aquifer analysis that "using wrong structural assumptions about the spatial variability of storativity showed significant, but not dramatic deviations in the estimated log-transmissivity fields."

[67] HT provides one method for estimating K variability that jointly fits all data and acknowledges the variable sensitivity of hydraulic measurements to spatially distributed hydraulic properties. As such, it does not make the "effective" homogeneous parameter assumptions that are made by traditional pumping test and slug test analyses, the meaning of which may be difficult to interpret [see, e.g., *Beckie and Harvey*, 2002; *Wu et al.*, 2005]. That said, hydraulic tomography requires a high degree of computational resources in addition to the installation of wells or multilevel samplers for measuring depth-dependent pressure changes.

[68] In cases where heterogeneity is predominantly 1-D (i.e., layered and only depth dependent), similar maps of heterogeneity may be obtained by using simpler methods,

Table 5. Parameter Values in True Model for Layered Aquifer, Analysis Case 5

	$\log_{10}(K)$ ($\log_{10}$(m s^{-1}))	$\log_{10}(S_s)$ ($\log_{10}$(1 m^{-1}))	$\log_{10}(S_y)$ (−)
Layer 1 (top)	−4.00	−6.00	−2.00
Layer 2	−2.00	−4.00	−1.00
Layer 3	−4.50	−5.50	−1.75
Layer 4 (bottom)	−2.50	−4.80	−1.25

such as analyzing core samples, multilevel slug tests, or direct push instrument responses. However, if aquifer heterogeneity has significant 2-D or 3-D variability, using these techniques may lead to incorrect inferences about connectivity between borehole locations [*Liu et al.*, 2007]. In addition, these techniques face other practical difficulties, e.g., direct push equipment can be limited by aquifer material type and penetration refusal depths, and analysis of core samples is dependent on core recovery. At the other end of the spectrum, tracer-based studies offer even more information than HT about 3-D connectivity when the tracer tests are analyzed tomographically [e.g., *Cirpka and Kitanidis*, 2001; *Pollock and Cirpka*, 2008, 2010], but may require time, instrumentation, and computational resources that are well beyond what is required by HT. Studies such as the one presented here can help site managers to assess the costs and value of hydraulic tomography relative to these other characterization methods.

[69] **Acknowledgments.** We gratefully acknowledge support for this research which was provided by NSF under grants EAR-0710949 and DMS-0934680, and by the US Army RDECOM ARL Army Research Office under grant W911NF-09-l-0534. In addition, the authors would like to thank the three anonymous reviewers and the Associate Editor (Walter Illman) for their insightful comments, which helped improve the quality of this work.

References

Barrash, W., and T. Clemo (2002), Heirarchical geostatistics and multifacies systems: Boise hydrogeophysical research site, Boise, Idaho, *Water Resour. Res.*, *38*(10), 1196, doi:10.1029/2002WR001436, a field study that may become the basis for future zonation research. Uses t-tests and Kolmogorov-Smirnov test to check the validity of zones found through composite neutron well log, GPR (ground penetrating radar), and other measurements. All delineations are manual (user created). Variograms are assumed for each of the geologic "facies."

Beckie, R., and C. F. Harvey (2002), What does a slug test measure: An investigation of instrument response and the effects of heterogeneity, *Water Resour. Res.*, *38*(12), 1290, doi:10.1029/2001WR001072.

Berg, S., and W. Illman (2011a), Capturing aquifer heterogeneity: Comparison of approaches through controlled sandbox experiments. *Water Resour. Res.*, *47*(9), W09514, doi:10.1029/2011WR010429.

Berg, S., and W. Illman (2011b), Three-dimensional transient hydraulic tomography in a highly heterogeneous glaciofluvial aquifer-aquitard system, *Water Resour. Res.*, *47*(10), W10507, doi: 10.1029/2011WR 010616.

Bohling, G. C. (2009), Sensitivity and resolution of tomographic pumping in an alluvial aquifer, *Water Resour. Res.*, *45*, W02420, doi:10.1029/2008WR007249.

Bohling, G. C., and J. J. Butler (2010), Inherent limitations of hydraulic tomography, *Ground Water*, *48*(6), 809–824.

Bohling, G. C., X. Zhan, J. J. Butler, and L. Zheng (2002), Steady shape analysis of tomographic pumping tests for characterization of aquifer heterogeneities, *Water Resour. Res.*, *38*(12), 1324, doi:10.1029/2001WR001176.

Bohling, G. C., J. J. Butler, X. Zhan, and M. D. Knoll (2007), A field assessment of the value of steady shape hydraulic tomography for characterization of aquifer heterogeneities, *Water Resour. Res.*, *43*, W05430, doi:10.1029/2006WR004932.

Brauchler, R., J.-T. Cheng, P. Dietrich, M. Everett, B. Johnson, R. Liedl, and M. Sauter (2007), An inversion strategy for hydraulic tomography: Coupling travel time and amplitude inversion, *J. Hydrol.*, *345*, 184–198.

Brauchler, R., R. Hu, T. Vogt, D. Al-Halbouni, T. Heinrichs, T. Ptak, and M. Sauter (2010), Cross-well slug interference tests: An effective characterization method for resolving aquifer heterogeneity, *J. Hydrol.*, *384*, 33–45.

Brauchler, R., R. Hu, P. Dietrich, and M. Sauter (2011), A field assessment of high-resolution aquifer characterization based on hydraulic travel time and hydraulic attenuation tomography, *Water Resour. Res.*, *47*, W03503, doi:10.1029/2010WR009635.

Butler, J. J., J. M. Healey, G. W. Mccall, E. J. Garnett, and S. P. I. Loheide (2002), Hydraulic tests with direct push equipment, *Ground Water*, *40*(1), 25–36.

Caers, J. (2003), History matching under a training image-based geological model constraints, *SPE J.*, *74716*, 218–226.

Cardiff, M. (2010), Authors' reply to comments on "A potential-based inversion of unconfined steady-state hydraulic tomography," *Ground Water*, *48*(3), 344–345.

Cardiff, M., and P. K. Kitanidis (2009), Bayesian inversion for facies detection: An extensible level set framework, *Water Resour. Res.*, *45*, W10416, doi:10.1029/2008WR007675.

Cardiff, M., W. Barrash, P. Kitanidis, B. Malama, A. Revil, S. Straface, and E. Rizzo (2009), A potential-based inversion of unconfined steady-state hydraulic tomography, *Ground Water*, *47*(2), 259–270.

Castagna, M., and A. Bellin (2009), A Bayesian approach for inversion of hydraulic tomographic data, *Water Resour. Res.*, *45*, W04410, doi:10.1029/2008WR007078.

Cirpka, O. A., and P. K. Kitanidis (2001), Sensitivities of temporal moments calculated by the adjoint-state method and joint inversing of head and tracer data, *Adv. Water Resour.*, *24*(1), 89–103.

Clemo, T. (2007), Modflow-2005 ground water model—User guide to the adjoint state based sensitivity process (adj), Tech. Rep., Boise State University.

Endres, A. L., J. P. Jones, and E. A. Bertrand (2007), Pumping-induced vadose zone drainage and storage in an unconfined aquifer: A comparison of analytical model predictions and field measurements, *J. Hydrol.*, *335*, 207–218.

Fienen, M. N., T. Clemo, and P. Kitanidis (2008), An interactive Bayesian geostatistical inverse protocol for hydraulic tomography, *Water Resour. Res.*, *44*, W00B01, doi:10.1029/2007WR006730.

Gottlieb, J., and P. Dietrich (1995), Identification of the permeability distribution in soil by hydraulic tomography, *Inverse Problems*, *11*, 353–360.

Hao, Y., T.-C. J. Yeh, J. Xiang, W. Illman, K. Ando, K.-C. Hsu, and C.-H. Lee (2008), Hydraulic tomography for detecting fracture zone connectivity, *Ground Water*, *46*(2), 183–192.

Harbaugh, A. (2005), Modflow-2005, the U.S. geological survey modular ground-water model—The ground-water flow process, Tech. Rep., USGS.

Huang, S.-Y., J.-C. Wen, T.-C. J. Yeh, W. Lu, H.-L. Juan, C.-M. Tseng, J.-H. Lee, and K.-C. Chang (2011), Robustness of joint interpretation of sequential pumping tests: Numerical and field experiments, *Water Resour. Res.*, *47*(10), W10530, doi:10.1029/2011WR010698.

Illman, W., X. Liu, and A. Craig (2007), Steady-state hydraulic tomography in a laboratory aquifer with deterministic heterogeneity: Multi-method and multiscale validation of hydraulic conductivity tomograms, *J. Hydrol.*, *341*, 222–234.

Illman, W., A. Craig, and X. Liu (2008), Practical issues in imaging hydraulic conductivity through hydraulic tomography, *Ground Water*, *46*(1), 120–132.

Illman, W., X. Liu, S. Takeuchi, T.-C. J. Yeh, K. Ando, and H. Saegusa (2009), Hydraulic tomography in fractured granite: Mizunami underground research site, Japan, *Water Resour. Res.*, *45*, W01406, doi:10.1029/2007WR006715.

Illman, W., S. J. Berg, X. Liu, and A. Massi (2010a), Hydraulic/partitioning tracer tomography for DNAPL source zone characterization: Small-scale sandbox experiments, *Environ. Sci. Technol.*, *44*(22), 8609–8614.

Illman, W., J. Zhu, A. J. Craig, and D. Yin (2010b), Comparison of aquifer characterization approaches through steady state groundwater model validation: A controlled laboratory sandbox study, *Water Resour. Res.*, *46*, W04502, doi:10.1029/2009WR007745.

Jacob, C. E. (1963), Determining the permeability of water-table aquifers, *U.S. Geol. Surv. Water Supply Paper*, 1536-I, pp. 245–271.

Kitanidis, P. K. (1995), Quasi-linear geostatistical theory for inversing, *Water Resour. Res.*, *31*(10), 2411–2419.

Kitanidis, P. K. (1996), On the geostatistical approach to the inverse problem, *Adv. Water Resour.*, *19*(6), 333–342.

Kitanidis, P. K., and E. Vomvoris (1983), A geostatistical approach to the inverse problem in groundwater modeling (steady state) and one-dimensional simulations, *Water Resour. Res.*, *19*(3), 677–690.

Kruseman, G., and N. deRidder (1990), Analysis and evaluation of pumping test data, Tech. Rep., International Institute for Land Reclamation and Improvement.

Kuhlman, K. L., A. C. Hinnell, P. K. Mishra, and T.-C. J. Yeh (2008), Basin-scale transmissivity and storativity estimation using hydraulic tomography, *Ground Water*, *46*(5), 706–715.

Li, W., W. Nowak, and O. A. Cirpka (2005), Geostatistical inverse modeling of transient pumping tests using temporal moments of drawdown, *Water Resour. Res.*, *41*, W08403, doi:10.1029/2004WR003874.

Li, W., A. Englert, O. A. Cirpka, J. Vanderborght, and H. Vereecken (2007), Two-dimensional characterization of hydraulic heterogeneity by multiple pumping tests, *Water Resour. Res.*, *43*, W04433, doi:10.1029/2006WR005333.

Li, W., A. Englert, O. A. Cirpka, and H. Vereecken (2008), Three-dimensional geostatistical inversion of flowmeter and pumping test data, *Ground Water*, *46*(2), 193–201.

Liu, S., J. T.-C. Yeh, and R. Gardiner (2002), Effectiveness of hydraulic tomography: Sandbox experiments, *Water Resour. Res.*, *38*(4), 1034, doi:10.1029/2001WR000338.

Liu, X., and P. K. Kitanidis (2011), Large-scale inverse modeling with an application in hydraulic tomograpy, *Water Resour. Res.*, *47*, W02501, doi:10.1029/2010WR009144.

Liu, X., W. Illman, A. Craig, J. Zhu, and T.-C. J. Yeh (2007), Laboratory sandbox validation of transient hydraulic tomography, *Water Resour. Res.*, *43*(5), W05404, doi:10.1029/2006WR005144.

Mishra, P., and S. Neuman (2010), Improved forward and inverse analyses of saturated-unsaturated flow toward a well in a compressible unconfined aquifer, *Water Resour. Res.*, *46*(7), W07508, doi:10.1029/2009WR008899.

Mishra, P., and S. Neuman (2011), Saturated-unsaturated flow to a well with storage in a compressible unconfined aquifer, *Water Resour. Res.*, *47*(5), W05553, doi:10.1029/2010WR010177.

Moench, A. (2008), Analytical and numerical analyses of an unconfined aquifer test considering unsaturated zone characteristics, *Water Resour. Res.*, *44*(6), W06409, doi:10.1029/2006WR005736.

Moench, A. F. (1994), Specific yield as determined by type-curve analysis of aquifer-test data, *Ground Water*, *32*(6), 949–957.

Narasimhan, T., and M. Zhu (1993), Transient flow of water to a well in an unconfined aquifer: Applicability of some conceptual models, *Water Resour. Res.*, *29*(1), 179–191.

Neuman, S. (1975), Analysis of pumping test data from anisotropic unconfined aquifers considering delayed gravity response, *Water Resour. Res.*, *11*(2), 329–342.

Ni, C.-F., T.-C. J. Yeh, and J.-S. Chen (2009), Cost-effective hydraulic tomography surveys for predicting flow and transport in heterogeneous aquifers, *Environ. Sci. Technol.*, *43*(10), 3720–3727.

Nowak, W., S. Tenkleve, and O. A. Cirpka (2003), Efficient computation of linearized cross-covariance and auto-covariance matrices of interdependent quantities, *Math. Geosci.*, *35*(1), 53–66.

Nwankwor, G., J. Cherry, and R. Gillham (1984), A comparative study of specific yield determinations for shallow sand aquifer, *Ground Water*, *22*(6), 764–772.

Pollock, D., and O. A. Cirpka (2008), Temporal moments in geoelectrical monitoring of salt tracer experiments, *Water Resour. Res.*, *44*, W12416, doi:10.1029/2008WR007014.

Pollock, D., and O. A. Cirpka (2010), Fully coupled hydrogeophysical inversion of synthetic salt tracer experiments, *Water Resour. Res.*, *46*, W07501, 10.1029/2009WR008575.

Snodgrass, M., and P. K. Kitanidis (1998), Transmissivity identification through multi-directional aquifer stimulation, *Stochastic Hydrol. Hydraul.*, *12*(5), 299–316.

Straface, S., C. Fallico, S. Troisi, E. Rizzo, and A. Revil (2007a), An inverse procedure to estimate transmissivity from heads and SP signals, *Ground Water*, *45*(4), 420–428.

Straface, S., T.-C. J. Yeh, J. Zhu, S. Troisi, and C. H. Lee (2007b), Sequential aquifer tests at a well field, Montalto Uffugo Scalo, Italy, *Water Resour. Res.*, *43*, W07432, doi:10.1029/2006WR005287.

Sun, A. Y., A. P. Morris, and S. Mohanty (2009), Sequential updating of multimodal hydrogeologic parameter fields using localization and clustering techniques, *Water Resour. Res.*, *45*, W07424, doi:10.1029/2008WR007443.

Tartakovsky, G., and S. Neuman (2007), Three-dimensional saturated-unsaturated flow with axial symmetry to a partially penetrating well in a compressible unconfined aquifer, *Water Resour. Res.*, *43*(1), W01410, doi:10.1029/2006WR005153.

Vasco, D. (2008), Zeroth-order inversion of transient pressure observations, *Inverse Problems*, *24*, 02513.

Vasco, D., and S. Finsterle (2004), Numerical trajectory calculations for the efficient inversion of transient flow and tracer observations, *Water Resour. Res.*, *40*, W01507, doi:10.1029/2003WR002362.

Vasco, D., and K. Karasaki (2001), Inversion of pressure observations: An integral formulation, *J. Hydrol.*, *253*, 27–40.

Vasco, D., and K. Karasaki (2006), Interpretation and inversion of low-frequency head observations, *Water Resour. Res.*, *42*, W05408, doi:10.1029/2005WR004445.

Vasco, D., A. Datta-Gupta, and J. C. S. Long (1997), Resolution and uncertainty in hydrologic characterization, *Water Resour. Res.*, *33*(3), 379–397.

Vasco, D., H. Keers, and K. Karasaki (2000), Estimation of reservoir properties using transient pressure data: An asymptotic approach, *Water Resour. Res.*, *36*(12), 3447–3465.

Wu, C.-M., T.-C. J. Yeh, J. Zhu, T. H. Lee, N.-S. Hsu, C.-H. Chen, and A. F. Sancho (2005), Traditional analysis of aquifer tests: Comparing apples to oranges?, *Water Resour. Res.*, *41*, W09402, doi:10.1029/2004WR003717.

Xiang, J., T.-C. J. Yeh, C.-H. Lee, K.-C. Hsu, and J.-C. Wen (2009), A simultaneous successive linear estimator and a guide for hydraulic tomography analysis, *Water Resour. Res.*, *45*, W02432, doi:10.1029/2008WR007180.

Yeh, J. T.-C., and S. Liu (2000), Hydraulic tomography: Development of a new aquifer test method, *Water Resour. Res.*, *36*(8), 2095–2105.

Yeh, T.-C. J., and J. Zhu (2007), Hydraulic/partitioning tracer tomography for characterization of dense nonaqueous phase liquid source zones, *Water Resour. Res.*, *43*, W06435, doi:10.1029/2006WR004877.

Yeh, T.-C. J., A. Gutjahr, and M. Jin (1995), An iterative cokriging-like technique for groundwater flow modeling, *Ground Water*, *33*(1), 33–41.

Yeh, T.-C. J., M. Jin, and S. Hanna (1996), An iterative stochastic inverse method: Conditional effective transmissivity and hydraulic head fields, *Water Resour. Res.*, *32*(1), 85–92.

Yin, D., and W. Illman (2009), Hydraulic tomography using temporal moments of drawdown recovery data: A laboratory sandbox study, *Water Resour. Res.*, *45*, W01502, doi:10.1029/2007WR006623.

Zhu, J., and J. T.-C. Yeh (2005), Characterization of aquifer heterogeneity using transient hydraulic tomography, *Water Resour. Res.*, *41*, W07028, doi:10.1029/2004WR003790.

Zhu, J., and T.-C. J. Yeh (2006), Analysis of hydraulic tomography using temporal moments of drawdown recovery data, *Water Resour. Res.*, *42*, W02403, doi:10.1029/2005WR004309.

Zimmerman, D., et al. (1998), A comparison of seven geostatistically based inverse approaches to estimate transmissivities for modeling advective transport by groundwater flow, *Water Resour. Res.*, *34*(6), 1373–1413.

W. Barrash, Center for Geophysical Investigation of the Shallow Subsurface (CGISS), Department of Geosciences, Boise State University, 1910 University Drive, MG-206, MS 1536, Boise, ID 83725, USA. (wbarrash@cgiss.boisestate.edu)

M. Cardiff, Center for Geophysical Investigation of the Shallow Subsurface (CGISS), Department of Geosciences, Boise State University, 1910 University Drive, MG-206, MS 1536, Boise, ID 83725, USA. (michaelcardiff@boisestate.edu)